J|A|C|S ARTICLES

Published on Web 04/27/2010

Stark Effects after Excited-State Interfacial Electron Transfer at Sensitized TiO_2 Nanocrystallites

Shane Ardo,[†] Yali Sun,[‡] Aaron Staniszewski,[†] Felix N. Castellano,*[,‡] and Gerald J. Meyer*[,†]

Departments of Chemistry and Materials Science and Engineering, Johns Hopkins University, 3400 North Charles Street, Baltimore, Maryland 21218, and Department of Chemistry and Center for Photochemical Sciences, Bowling Green State University, Bowling Green, Ohio 43403

Received November 18, 2009; E-mail: castell@bgnet.bgsu.edu; meyer@jhu.edu

Abstract: Photophysical studies were performed with $[Ru(dtb)_2(dcb)](PF_6)_2$ and *cis*-$Ru(dcb)(dnb)(NCS)_2$, where dtb is 4,4′-$(C(CH_3)_3)_2$-2,2′-bipyridine, dcb is 4,4′-$(COOH)_2$-2,2′-bipyridine, and dnb is 4,4′-$(CH_3(CH_2)_8)_2$-2,2′-bipyridine), anchored to anatase TiO_2 particles (∼15 nm in diameter) interconnected in a mesoporous, 10 μm thick film immersed in Li^+-containing CH_3CN electrolytes with iodide or phenothiazine donors. Pulsed-laser excitation resulted in rapid excited-state injection and donor oxidation to yield $TiO_2(e^-)$s and oxidized donors, while the metal-to-ligand charge-transfer (MLCT) absorption spectrum of the Ru(II) coordination compounds differed from that which was initially excited. The spectral data were consistent with an underlying Stark effect and indicated that the surface electric field was not completely screened from the molecular sensitizer. The magnitude of the electric field was estimated to be ∼270 MV/m from Li^+ titration experiments, corresponding to a ∼40 mV potential drop. With iodide donors, the amplitude of the Stark effect decreased over time periods where charge recombination was absent, behavior attributed to "screening" of the electric field by interfacial ionic reorganization. The screening kinetics were nonexponential but were well described by the Kohlrausch−Williams−Watts model, from which a characteristic rate constant, τ_o^{-1}, of $\sim 1.5 \times 10^5$ s^{-1} was abstracted. At least seven other sensitizers and five different cations, as well as on SnO_2 nanoparticle films, exhibited similar transient absorption behavior with iodide donor molecules indicating that the effect was quite general. In the presence of phenothiazine donors (or in the absence of an external donor), there was no clear evidence for screening, and the Stark effect disappeared concurrent with interfacial charge recombination. Complementary spectroelectrochemical studies of these same sensitized films displayed similar absorption spectra when the TiO_2 thin film was partially reduced with a forward bias. Spectral modeling in the absence of donor molecules as well as studies of TiO_2 thin films sensitized with two different Ru(II) compounds demonstrated that the electric field created by excited-state injection from one sensitizer influenced the absorption spectra of other sensitizers that had not undergone photoinduced electron injection.

It has been 18 years since Grätzel, O'Regan, and Anderson first introduced thin films composed of ∼20 nm anatase TiO_2 particles interconnected in a mesoporous 10 μm thick film for applications in dye-sensitized solar cells.[1,2] Global conversion efficiencies greater than 11% have now been confirmed by several certified laboratories.[3−7] Ruthenium polypyridyl compounds, such as N3, *cis*-$Ru(dcb)_2(NCS)_2$, where dcb is 4,4′-$(COOH)_2$-2,2′-bipyridine, are generally the optimum sensitizers for this application due to their high stability and broad spectral light harvesting.[8] In sunlight, such sensitizers rapidly and quantitatively undergo three consecutive charge-transfer reactions: (1) metal-to-ligand charge transfer (MLCT) excitation, (2) excited-state electron injection into TiO_2, and (3) reduction through iodide oxidation. In principle, the sensitizer is now "regenerated" and can repeat the "sensitization cycle" of light absorption, excited-state injection, and iodide oxidation as shown in Scheme 1. When irradiated with 1 sun of air mass 1.5 sunlight, each sensitizer repeats this cycle about twice per second, on average.[9] Under short-circuit conditions, the injected electrons are rapidly and quantitatively collected in an external circuit. At open circuit, current does not flow, and the concentration of electrons injected into the TiO_2 nanoparticles, $TiO_2(e^-)$s, increases to a steady-state value. At the condition of maximum power generation, roughly 10 injected electrons have been estimated to reside in each TiO_2 nanocrystallite.[10]

[†] Johns Hopkins University.
[‡] Bowling Green State University.

(1) O'Regan, B.; Moser, J.; Anderson, M.; Grätzel, M. *J. Phys. Chem.* **1990**, *94*, 8720–8726.
(2) O'Regan, B.; Grätzel, M. *Nature* **1991**, *353*, 737–740.
(3) Seigo, I.; Md. Khaja, N.; Paul, L.; Pascal, C.; Raphaël, C.; Péter, P.; Marie, J.; Andreas, K.; Shaik, M. Z.; Michael, G. *Prog. Photovolt. Res. Appl.* **2006**, *14*, 589–601.
(4) Martin, A. G.; Keith, E.; Yoshihiro, H.; Wilhelm, W. *Prog. Photovolt. Res. Appl.* **2009**, *17*, 85–94.
(5) Gao, F.; Wang, Y.; Shi, D.; Zhang, J.; Wang, M.; Jing, X.; Humphry-Baker, R.; Wang, P.; Zakeeruddin, S. M.; Grätzel, M. *J. Am. Chem. Soc.* **2008**, *130*, 10720–10728.
(6) Chiba, Y.; Islam, A.; Watanabe, Y.; Komiya, R.; Koide, N.; Han, L. *Jpn. J. Appl. Phys., Part 2* **2006**, *45*, L638-L640.
(7) Kroon, J. M.; et al. *Prog. Photovolt. Res. Appl.* **2007**, *15*, 1–18.
(8) Nazeeruddin, M. K.; Kay, A.; Rodicio, I.; Humphry-Baker, R.; Mueller, E.; Liska, P.; Vlachopoulos, N.; Grätzel, M. *J. Am. Chem. Soc.* **1993**, *115*, 6382–6390.
(9) Grätzel, M. *Cattech* **1999**, *3*, 4–17.

 10.1021/ja909781g

Scheme 1. Light Absorption, Excited-State Injection, and Iodide Oxidation Termed the "Sensitization Cycle," as Shown for a $Ru(dtb)_2(dcb)^{2+}$-Sensitized TiO_2 Nanocrystalline Thin Film, where dtb is 4,4′-$(C(CH_3)_3)_2$-2,2′-bipyridine

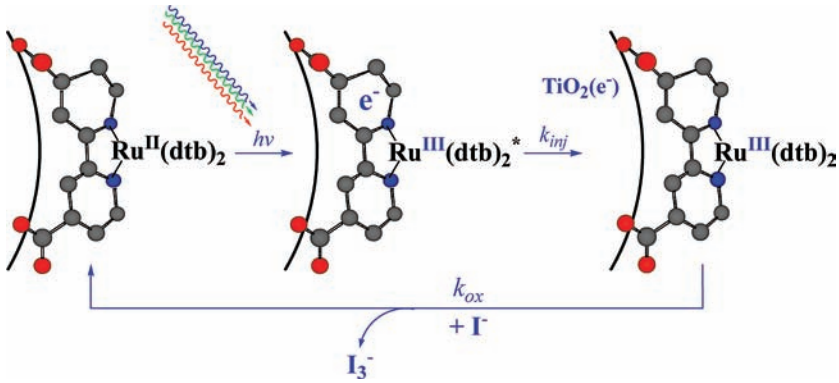

The influence of the $TiO_2(e^-)$ concentration on the individual steps of the sensitization cycle is generally unknown and represents an active area of investigation. Furthermore, aside from these Faradaic charge-transfer reactions, there exist non-Faradaic processes that are known to accompany interfacial electron transfer. For example, it has been recognized for some time that Li^+ reversibly intercalates or binds to the surface of reduced anatase TiO_2 nanocrystallites.[11−15] Similarly, and possibly related, is the cursorily understood phenomenon where prolonged light soaking of an assembled dye-sensitized solar cell yields increased power-conversion efficiencies.[16−19] By further inspection, one realizes that the overall sensitization cycle shown schematically is merely *redox* regenerative. That is, the sensitizer does return to its initial formal oxidation state; however, all interfacial-related processes may not have reset.

A recent communication reported that excited-state injection and sensitizer regeneration resulted in the formation of Ru(II) sensitizers that were in different environments than those that were present before light absorption.[20] The initial environment was restored only after slow micro- to millisecond cation transfer and interfacial charge recombination had occurred. Once the spectroscopic signatures associated with this process were identified, they were evident in previously published work for N3- and $[Ru(bpy)_2(dcb)]^{2+}$-sensitized metal oxides.[21,22] These transient absorption features were often subtle and may have been attributed to noise. However, the fact that they could be reproduced and modeled in other laboratories indicated that they were significant. In a more recent 2009 paper, Hagfeldt, Boschloo, and colleagues reported the spectroelectrochemical properties of perylene-sensitized TiO_2 thin-film electrodes.[23] Reduction of the anatase nanocrystallites resulted in significant and reversible changes to the perylene visible absorption spectrum. Similar spectral features were observed by photoinduced absorption spectroscopy in the absence of a supporting electrolyte. A unique aspect of these perylene sensitizers was that they were neutral compounds that did not contain ionizable functional groups. Therefore, the sensitized thin film was not intentionally exposed to protons or Lewis-acidic cations. The origin of the spectral changes was attributed to an energetic shift in the lowest-unoccupied molecular orbital due to the increased $TiO_2(e^-)$ density that resulted from the forward bias or sensitization.

Herein we report systematic studies designed to better understand how excited-state electron injection influences the spectroscopic properties of sensitizers confined to mesoporous nanocrystalline thin films. Experiments performed with dicationic Ru(II) tris-diimine and neutral Ru(II) bis-diimine bis-isothiocyanato sensitizers in the presence and absence of electron donors and with selected electrolytes have provided new insights into the underlying mechanism. In the course of this work, direct spectroscopic evidence for a previously unidentified Stark effect,[24] where the UV−vis absorption spectrum is perturbed by an electric field, and subsequent screening process were quantified. Studies of TiO_2 thin films cosensitized with two different Ru(II) compounds indicated that ground-state sensitizers that were not photoexcited were influenced by electrons injected from neighboring sensitizers that had undergone excited-state interfacial electron transfer, thus supporting a conclusion that the observed spectral shifts were indeed electric-field induced. Although it is often tacitly assumed that the high ionic strength electrolytes and large permittivity of the dye-sensitized solar cell components results in little-to-no internal electric fields and electrical potential drops, the presence of this newly understood phenomenon suggests otherwise.

Experimental Section

Materials. All chemicals were reagent grade or better unless otherwise specified and were used without further purification. The following reagents and substrates were used as received from the

(10) O'Regan, B. C.; Durrant, J. R. *Acc. Chem. Res.* **2009**, *42*, 1799–1808.
(11) Pelet, S.; Moser, J. E.; Grätzel, M. *J. Phys. Chem. B* **2000**, *104*, 1791–1795.
(12) Enright, B.; Redmond, G.; Fitzmaurice, D. *J. Phys. Chem.* **1994**, *98*, 6195–6200.
(13) Ardo, S.; Meyer, G. J. *Chem. Soc. Rev.* **2009**, *38*, 115–164.
(14) Lindstrom, H.; Sodergren, S.; Solbrand, A.; Rensmo, H.; Hjelm, J.; Hagfeldt, A.; Lindquist, S. E. *J. Phys. Chem. B* **1997**, *101*, 7710–7716.
(15) Lindstrom, H.; Sodergren, S.; Solbrand, A.; Rensmo, H.; Hjelm, J.; Hagfeldt, A.; Lindquist, S. E. *J. Phys. Chem. B* **1997**, *101*, 7717–7722.
(16) Wang, Q.; Zhang, Z.; Zakeeruddin, S. M.; Grätzel, M. *J. Phys. Chem. C* **2008**, *112*, 7084–7092.
(17) O'Regan, B.; Schwartz, D. T. *Chem. Mater.* **1998**, *10*, 1501–1509.
(18) Gregg, B. A.; Chen, S.-G.; Ferrere, S. *J. Phys. Chem. B* **2003**, *107*, 3019–3029.
(19) Ferrere, S.; Gregg, B. A. *J. Phys. Chem. B* **2001**, *105*, 7602–7605.
(20) Staniszewski, A.; Ardo, S.; Sun, Y.; Castellano, F. N.; Meyer, G. J. *J. Am. Chem. Soc.* **2008**, *130*, 11586–11587.
(21) Montanari, I.; Nelson, J.; Durrant, J. R. *J. Phys. Chem. B* **2002**, *106*, 12203–12210.
(22) Nasr, C.; Hotchandani, S.; Kamat, P. V. *J. Phys. Chem. B* **1998**, *102*, 4944–4951.
(23) Cappel, U. B.; Gibson, E. A.; Hagfeldt, A.; Boschloo, G. *J. Phys. Chem. C* **2009**, *113*, 6275–6281.
(24) Stark, J. *Nature* **1913**, *92*, 401.

indicated commercial suppliers: dichloro(*p*-cymene)ruthenium(II) dimer (Aldrich); 4,4′,4″-*tert*-butyl-2,2′,2″-terpyridine (^{t}Bu$_3$tpy; Aldrich); 4,4′-di-*tert*-butyl-2,2′-bipyridine (dtb; Aldrich); 4,4′-dimethyl-2,2′-bipyridine (Aldrich); 4,4′-dinonyl-2,2′-dipyridyl (dnb; Aldrich); ruthenium(III) chloride hydrate (Aldrich), potassium thiocyanate (Acros); lithium chloride (Fisher); 1-methylimidazole (Aldrich, 99%); 1-iodopropane (Aldrich, 99%); acetonitrile (Burdick & Jackson, spectrophotometric grade); toluene (OmniSolv, 99.99%); lithium perchlorate (Aldrich, 99.99%); *n*-tetrabutylammonium perchlorate (TBAP; Fluka, >99.9%); *n*-tetrabutylammonium chloride (TBACl; Sigma Aldrich, 98%); *n*-tetrabutylammonium iodide (TBAI; Aldrich, >99% or Fluka, >98%); phenothiazine (PTZ; Aldrich, >98%); magnesium(II) perchlorate (Aldrich, reagent grade); copper(II) perchlorate hexahydrate (Alfa Aesar, reagent grade); silver nitrate (Bioanalytical Scientific Instruments, Inc.); guanidine thiocyanate (Sigma, >99%); hydrochloric acid (Fisher Scientific, 37.2% aqueous solution); argon gas (Airgas, >99.998%); nitrogen gas (Airgas, >99.999%); oxygen gas (Airgas, industrial grade); titanium(IV) isopropoxide (Sigma-Aldrich, 97%); zirconium(IV) propoxide (Aldrich, 70 wt % solution in 1-propanol); SnO_2 colloidal solution (Alfa Aesar, 15% in water); fluorine-doped SnO_2-coated glass (FTO; Hartford Glass Co., Inc., 2.3 mm thick, 15 Ohm/□); microscope slides (Fisher Scientific, 1 mm thick); and polished CaF_2 windows (International Crystal Laboratories, 2 mm thick).

Preparations. The following ligands and metal complexes were prepared by adaptation of relevant literature procedures: 4,4′-dicarboxy-2,2-bipyridine (dcb),[25] 4,4′-diethyl ester-2,2′-bipyridine (deeb),[26] *cis*-Ru(DMSO)$_4$Cl$_2$,[27] *cis*-Ru(dtb)$_2$Cl$_2$·2H$_2$O,[28] and [Ru(dtb)$_2$(deeb)](PF$_6$)$_2$.[29] Z907 was synthesized precisely as the published one-pot procedure departing from [Ru(*p*-cymene)Cl$_2$]$_2$.[30,31] The other sensitizers employed were available from previous studies: [Ru(bpy)$_2$(dcb)](PF$_6$)$_2$,[32] where bpy is 2,2′-bipyridine, [Ru(bpy)$_2$(4-CH$_3$-4′-COOH-bpy)](PF$_6$)$_2$,[33] [Ru(deeb)$_3$](PF$_6$)$_2$[34] and [Os(bpy)$_2$(deeb)](PF$_6$)$_2$.[35] ^{1}H NMR and ^{13}C NMR spectra were recorded on a Bruker Avance 300 (300 MHz) or Avance 400 (400 MHz) Fourier transform NMR spectrometer. MALDI-TOF mass spectra were measured using a Bruker-Daltonics Omniflex spectrometer. The attenuated total reflectance (ATR) Fourier transform infrared (FTIR) spectra of reaction products were recorded on a Thermo Scientific Nicolet IR200 spectrophotometer.

4,4′-Dicarboxy-2,2′-bipyridine (dcb).[25] In a 500 mL round-bottom flask equipped with a magnetic stirrer, 4,4′-dimethyl-2,2′-bipyridine (8 g, 0.04 mol) was dissolved in 100 mL of sulfuric acid at room temperature. The solution was cooled to 0 °C in an ice bath, and chromium trioxide (26 g, 0.26 mol) was added in small portions over 2 h with continuous stirring. The mixture turned red first, then bluish green. After the addition of chromium trioxide was complete, the mixture was heated to 75 °C and maintained at this temperature for 4 h. Subsequently, the mixture was stirred at room temperature for 10 h. The reaction mixture was poured into a large beaker containing ice and water, which was continuously stirred, obtaining a dark solution containing a yellowish green precipitate. The precipitate was vacuum filtered and washed with water several times. The yellowish powder obtained was dissolved in aqueous potassium hydroxide. The blue-green insoluble powder was filtered off, and the filtrate was acidified with concentrated hydrochloric acid, forming a white precipitate, which was filtered and washed with water, followed by diethyl ether. The white solid product was dried under vacuum to obtain the title compound, which was used without further purification (7.2 g, 74% yield).

4,4′-Diethyl ester-2,2′-bipyridine (deeb).[26] To 36 mL of thionyl chloride ($SOCl_2$) at room temperature was added dcb (7.2 g, 29.5 mmol). The mixture was refluxed overnight until the solution clarified. The excess thionyl chloride was removed by rotary evaporation yielding the acid chloride intermediate. To the solid residue was added 200 mL of absolute ethanol (anhydrous), and the mixture was refluxed overnight. Half of the ethanol was removed, and the resulting precipitate was collected by vacuum filtration. The crude product was recrystallized using absolute ethanol yielding the pure white title compound (7.0 g, 79% yield). ^{1}H NMR (300 MHz, $CDCl_3$): δ 8.95 (d, J = 1.5 Hz, 2H), 8.87 (d, J = 5.1 Hz, 2H), 7.92 (dd, J_1 = 5.1 Hz, J_2 = 1.5 Hz, 2H), 4.46 (q, J = 7.2 Hz, 4H), 1.45 (t, J = 7.2 Hz, 6H). EI-MS: m/z 300 $[M]^+$, 255 $[M - OC_2H_5]^+$, 228 $[M - COOC_2H_5]^+$ base peak, 200 $[M - COOC_2H_5 - C_2H_5]^+$.

[Ru(^{t}Bu$_3$tpy)(dcb)(NCS)](PF$_6$). Dichloro(*p*-cymene)ruthenium(II) dimer (109 mg, 0.18 mmol) and ^{t}Bu$_3$tpy (4,4′,4″-(C(CH$_3$)$_3$)$_3$-2,2′:6′,2″-terpyridine; 145 mg, 0.36 mmol) were dissolved in 50 mL of DMF. The solution was heated to 60 °C under argon in the dark for 4 h with constant stirring. The dcb (88 mg, 0.36 mmol) ligand was added, and the temperature was increased to 140 °C, which was maintained for an additional 4 h. Next, an excess amount of NH_4NCS (411 mg, 5.4 mmol) was added to the reaction mixture, which was maintained at 140 °C for an additional 4 h. After the reaction mixture was cooled to room temperature, most of the solvent was removed by using a rotary evaporator connected to a vacuum pump. Saturated aqueous NH_4PF_6 solution was added dropwise to the DMF residue producing an insoluble solid, which was collected on a sintered glass crucible by suction filtration. The crude compound was dissolved in methanol containing a few drops of chloroform. This solution was passed through a Sephadex LH-20 column using methanol as the eluent. The primary band was collected and concentrated (291 mg, 85% yield). ^{1}H NMR (300 MHz, $CHCl_3$ + CD_3OD): δ 9.77 (d, J = 5.7 Hz, 1H), 9.10 (s, 1H), 8.88 (s, 1H), 8.32 (dd, J_1 = 1.5 Hz, J_2 = 6 Hz, 1H), 8.26 (s, 2H), 8.11 (s, 2H), 7.43 (d, J = 6 Hz, 1H), 7.31 (d, J = 6 Hz, 2H), 7.16 (dd, J_1 = 1.8 Hz, J_2 = 6 Hz, 2H), 7.05 (d, J = 5.7 Hz, 1H), 1.60 (s, 9H), 1.29 (s, 18H). ^{13}C NMR (75 MHz, $CHCl_3$ + CD_3OD): δ 167.46, 166.81, 163.43, 161.71, 158.75, 158.46, 157.39, 157.05, 153.22, 152.19, 151.30, 143.55, 141.25, 134.45, 127.03, 126.48, 125.42, 123.76, 123.71, 121.60, 120.53, 36.75, 35.92, 31.07, 30.52. MALDI-MS (TOF): m/z 805.44 ($M^+ - PF_6^-$). FTIR (ATR): 2963 (s), 2874 (m), 2102 (s), 1716 (s), 1610 (s), 1541 (m), 1459 (m), 1367 (s), 1251 (s), 831 (vs).

***cis*-Ru(dtb)$_2$Cl$_2$·2H$_2$O.**[28] $RuCl_3$·3H$_2$O (0.52 g, 2.0 mmol), dtb (4,4′-(C(CH$_3$)$_3$)$_2$-2,2′-bipyridine; 1.07 g, 4.0 mmol), and an excess amount of lithium chloride (0.56 g, 13.3 mmol) were refluxed in 5 mL of DMF under argon in the dark for 6 h. After the reaction mixture was cooled to room temperature, ~15 mL of acetone was added, and the resultant solution was put into the refrigerator overnight. The mixture was filtered under vacuum to obtain a dark green-black powder, which was washed with water and diethyl ether (1.04 g, 70% yield). MALDI-MS (TOF): m/z 708.97 $[M]^+$, 673.47 $[M - Cl^-]^+$.

[Ru(dtb)$_2$(deeb)](PF$_6$)$_2$.[29] To a round-bottom flask containing deaerated ethanol−water (30 mL, 1:1) were added *cis*-Ru(dtb)$_2$Cl$_2$·2H$_2$O (343 mg, 0.46 mmol) and deeb (141 mg, 0.47 mmol). The mixture was refluxed under argon in the dark for 20 h. The solvent was removed by rotary evaporator under vacuum. Cold

(25) Garelli, N.; Vierling, P. *J. Org. Chem.* **2002**, *57*, 3046–3051.
(26) Sprintschnik, G.; Sprintschnik, H. W.; Kirsch, P. P.; Whitten, D. G. *J. Am. Chem. Soc.* **2002**, *99*, 4947–4954.
(27) Evans, I. P.; Spencer, A.; Wilkinson, G. *J. Chem. Soc., Dalton Trans.* **1973**, 204–209.
(28) Sullivan, B. P.; Salmon, D. J.; Meyer, T. J. *Inorg. Chem.* **2002**, *17*, 3334–3341.
(29) Liu, F.; Meyer, G. J. *Inorg. Chem.* **2005**, *44*, 9305–9313.
(30) Wang, P.; Zakeeruddin, S. M.; Moser, J. E.; Nazeeruddin, M. K.; Sekiguchi, T.; Grätzel, M. *Nat. Mater.* **2003**, *2*, 402–407.
(31) Nazeeruddin, M. K.; Zakeeruddin, S. M.; Lagref, J. J.; Liska, P.; Comte, P.; Barolo, C.; Viscardi, G.; Schenk, K.; Grätzel, M. *Coord. Chem. Rev.* **2004**, *248*, 1317–1328.
(32) Morris, A. J.; Meyer, G. J. *J. Phys. Chem. C* **2008**, *112*, 18224–18231.
(33) Meyer, T. J.; Meyer, G. J.; Pfennig, B. W.; Schoonover, J. R.; Timpson, C. J.; Wall, J. F.; Kobusch, C.; Chen, X.; Peek, B. M. *Inorg. Chem.* **2002**, *33*, 3952–3964.
(34) Gardner, J. M. Thesis, Johns Hopkins University, 2009.
(35) Higgins, G. T.; Bergeron, B. V.; Hasselmann, G. M.; Farzad, F.; Meyer, G. J. *J. Phys. Chem. B* **2006**, *110*, 2598–2605.

water (20 mL) was added to the solid residue. The mixture was filtered under vacuum, and the filtrate was collected. A saturated NH_4PF_6 aqueous solution was added dropwise to the filtrate and a precipitate formed immediately. The precipitate was collected on a fine frit and was purified over alumina using acetonitrile−ether (1:1) as the eluent (509 mg, 90% yield). ^{1}H NMR (300 MHz, CD_3CN): δ 9.01 (d, $J = 1.5$ Hz, 2H), 8.48−8.45 (m, 4H), 7.89 (d, $J = 6$ Hz, 2H), 7.82 (dd, $J_1 = 1.5$ Hz, $J_2 = 6$ Hz, 2H), 7.55−7.50 (m, 4H), 7.43−7.32 (m, 4H), 4.44 (q, $J = 7.2$ Hz, 4H), 1.40−1.39 (m, 42H, ^{t}Bu + $-CH_2CH_3$ protons). ^{13}C NMR (75 MHz, CD_3CN): δ 164.97, 164.48, 164.00, 158.83, 157.47, 157.37, 153.55, 153.49, 152.03, 151.60, 139.33, 138.97, 127.34, 125.76, 125.63, 124.49, 124.43, 122.61, 63.56, 36.32, 36.30, 30.41, 30.38, 14.39. MALDI-MS (TOF): m/z 1083.54 $[M - PF_6^-]^+$, 938.60 $[M - 2PF_6^-]^+$.

$[Ru(dtb)_2(dcb)](PF_6)_2$. $[Ru(dtb)_2(deeb)](PF_6)_2$ (172 mg, 0.14 mmol) and NaOH (16 mg, 0.4 mmol) were added to a solution containing 10 mL of absolute ethanol and 50 mL of H_2O; this mixture was refluxed in the dark for 10 h. After the solution was cooled to room temperature, it was acidified to pH ∼1−2. The resulting precipitate was collected on a fine frit, washed with copious amounts of water followed by Et_2O, and finally dried under vacuum (161 mg, 98% yield). ^{1}H NMR (300 MHz, CD_3CN): δ 9.75 (s, 2H), 8.46 (dd, $J_1 = 1.5$ Hz, $J_2 = 5.4$ Hz, 4H), 7.80 (m, 4H), 7.54 (m, 4H), 7.40 (dd, $J_1 = 1.8$ Hz, $J_2 = 6$ Hz, 2H), 7.30 (dd, $J_1 = 1.8$ Hz, $J_2 = 6$ Hz, 2H), 1.39 (s, 18H), 1.36 (s, 18H). ^{13}C NMR (75 MHz, CD_3CN): δ 165.72, 163.99, 158.89, 157.60, 157.56, 153.28, 152.09, 151.68, 140.88, 127.68, 125.76, 125.71, 124.90, 122.63, 118.30, 36.37, 36.35, 30.49, 30.47. MALDI-MS (TOF): m/z 1027.55 $[M - PF_6^-]^+$, 882.59 $[M - 2PF_6^-]^+$. FTIR (ATR): 2961 (w), 1719 (m), 1614 (m), 1546 (m), 1479 (m), 1411 (m), 1368 (m), 1317 (m), 1248 (m).

***cis*-$Ru(dcb)_2(NCS)_2$ (N3).** To 40 mL of DMF were added *cis*-$Ru(DMSO)_4Cl_2$ (300 mg, 0.62 mmol) and 1 equiv of dcb (151.6 mg, 0.62 mmol). After the mixture was heated at 60 °C under argon in the dark for 4 h, a second equivalent of dcb (151.6 mg, 0.62 mmol) was added. This mixture was heated to reflux for 4 h. Next, an excess amount of NH_4NCS (708 mg, 9.3 mmol) was added to the solution, which was refluxed for another 4 h. After the solution was cooled to room temperature, the DMF was removed under vacuum. Water (100 mL) was added to dissolve the soluble impurities. The remaining solid was collected by filtration. Finally, methanol was used to dissolve the collected product, which was subsequently filtered and stripped on a rotary evaporator. This process was repeated two additional times to yield the title compound (306 mg, 70% yield). ^{1}H NMR (300 MHz, DMSO-d_6): δ 9.42 (d, $J = 5.7$ Hz, 2H), 9.16 (s, 2H), 9.00 (s, 2H), 8.36 (dd, $J_1 = 1.2$ Hz, $J_2 = 5.7$ Hz, 2H), 7.78 (d, $J = 5.7$ Hz, 2H), 7.59 (dd, $J_1 = 1.2$ Hz, $J_2 = 5.7$ Hz, 2H). ^{13}C NMR (75 MHz, DMSO-d_6): δ 165.77, 165.34, 159.16, 157.70, 153.67, 153.39, 139.12, 138.35, 135.11, 126.82, 125.75, 123.58, 123.26. MALDI-MS (TOF): m/z 706.10 $[M]^+$.

1-*n*-Propyl-3-methylimidazolium Iodide. The ionic liquid was synthesized according to a previously published procedure and yielded a yellow oil (14.7 g, 92% yield).[36,37] ^{1}H NMR (300 MHz, $CDCl_3$): δ 9.80 (s, 1H), 7.65−7.69 (dd, 4H), 4.30 (t, 2H), 4.09 (s, 3H), 1.92−1.99 (m, 2H), 0.95 (t, 3H).

Sensitized Metal Oxide Thin Film (Electrode). Transparent TiO_2 nanocrystallites (anatase, ∼15 nm in diameter) and ZrO_2 nanoparticles were prepared by hydrolysis of the appropriate precursors (Ti(*i*-OPr)$_4$ or Zr(OPr)$_4$) using a sol−gel technique previously described in the literature.[38] The sols were cast as mesoporous thin films (∼10 μm thick) by doctor blading onto glass microscope slides for spectroscopic measurements, transparent FTO conductive substrates for electrochemical measurements, and polished CaF_2 windows for transmission-mode infrared measurements. Scotch tape was employed as a spacer. In all cases, the thin films were annealed at 420 °C for 30 min under O_2 flow.

Transparent SnO_2 thin films were prepared from a stock colloidal SnO_2 solution by a previously described method.[39] Thin films were cast via spin coating followed by thermal annealing at 450 °C for 30 min under O_2 flow.

Sensitization was achieved by immersing the supported thin films in sensitizer solutions (mM concentrations) for hours to days depending on the desired surface coverage and the rate at which the particular sensitizer reacted with the surface. Films were then soaked in the neat solvent that was used for the sensitizer binding for 5−10 min followed by a thorough washing with the experimental solvent. Unless noted otherwise, the thin films were sensitized to roughly maximum surface coverage, $\Gamma \sim 7 \times 10^{-8}$ mol/cm^2, which was calculated by a previously published method.[40] Briefly, the extinction coefficient at the maximum of the MLCT transition was assumed to be the same in solution *and on the* surface, in the appropriate comparative states just described. This value was used along with the modified Beer−Lambert Law formula to calculate a macroscopic surface coverage by $A = \varepsilon\Gamma 1000$. The samples were then quickly transferred to a standard 1 cm square quartz cuvette containing the experimental solution and were positioned diagonally (for microscope slide-supported films) or parallel (for FTO-supported films) in the cuvette. For transient absorption and electrochemical studies, the cuvettes containing the sample and electrolyte solution were purged with Ar gas for at least 30 min prior to experimentation, premoistened with the same electrolyte solution.

Spectroscopy. UV−vis Absorption. Steady-state UV−vis absorbance spectra were obtained on a Varian Cary 50 spectrophotometer at room temperature.

Nanosecond transient absorption measurements were obtained with an apparatus similar to that which has been previously described.[41] Briefly, samples were excited by a pulsed Nd:YAG laser (Quantel USA (BigSky) Brilliant B; 5−6 ns full width at half-maximum (fwhm), 1 Hz, ∼10 mm in diameter) tuned to 532 or 355 nm with the appropriate nonlinear optics. An H_2 Raman shifter (∼400 psi) was employed in order to obtain Stokes-shifted 683 or 416 nm excitation or anti-Stokes-shifted 436 nm excitation. The excitation fluence was measured by a thermopile power meter (Molectron) and was typically 3−4 mJ/pulse so that the absorbed fluence was typically <1 mJ/pulse, unless noted otherwise. A 150 W xenon arc lamp served as the probe beam (Applied Photophysics) and was aligned orthogonal to the laser excitation light. For detection at sub-100 microsecond time scales the lamp was pulsed with 100 V. Detection was achieved with a monochromator (Spex 1702/04) optically coupled to an R928 photomultiplier tube (Hamamatsu). Transient data was acquired on a computer-interfaced digital oscilloscope (LeCroy 9450, Dual 350 MHz) with 2.5 ns resolution terminated at 50 Ω for sub-100 microsecond data acquisition; for longer time scales, the signal was terminated with a 10 kΩ resistor and bandwidth limited at 80 MHz. The overall instrument response time was ∼10 ns. Typically, 20−60 laser pulses were averaged at each observation wavelength over the range 390−800 nm, at 10 nm intervals. Full spectra were generated by averaging 2−40 points on either side of the desired time value in order to help minimize noise in the raw data.

Infrared Absorption. FTIR absorbance spectra were obtained using a Thermo Scientific Nicolet Nexus 670 spectrophotometer. A 25 μm path length solution flow cell was employed using two CaF_2 windows: one with a sensitized thin film and the other without

(36) Leadbeater, N. E.; Torenius, H. M. *J. Org. Chem.* **2002**, *67*, 3145–3148.
(37) Leadbeater, N. E.; Torenius, H. M.; Tye, H. *Tetrahedron* **2003**, *59*, 2253–2258.
(38) Heimer, T. A.; D'Arcangelis, S. T.; Farzad, F.; Stipkala, J. M.; Meyer, G. J. *Inorg. Chem.* **1996**, *35*, 5319–5324.
(39) Bergeron, B. V.; Marton, A.; Oskam, G.; Meyer, G. J. *J. Phys. Chem. B* **2004**, *109*, 937–943.
(40) Trammell, S. A.; Meyer, T. J. *J. Phys. Chem. B* **1999**, *103*, 104–107.
(41) Argazzi, R.; Bignozzi, C. A.; Heimer, T. A.; Castellano, F. N.; Meyer, G. J. *Inorg. Chem.* **1994**, *33*, 5741–5749.

Scheme 2. Ru(II) sensitizers and their abbreviations

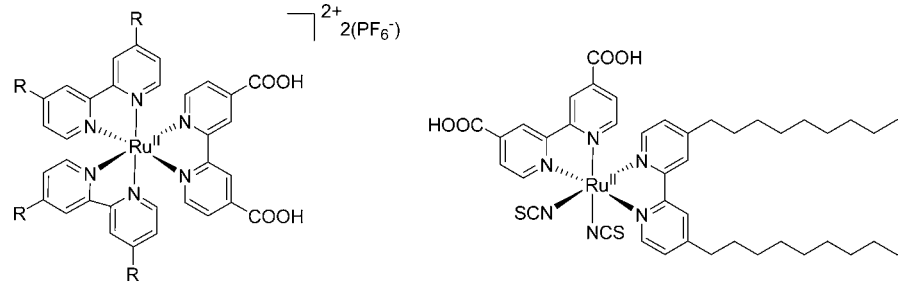

R = ^{t}Bu, [Ru(dtb)$_2$(dcb)](PF$_6$)$_2$
R = H, [Ru(bpy)$_2$(dcb)](PF$_6$)$_2$

cis-Ru(dnb)(dcb)(NCS)$_2$
(Z907)

a thin film.[42] The measurements were made in transmission mode under an N_2 atmosphere, and the spectra were averaged for 256 scans with 4 cm^{-1} resolution.

Photoluminescence. Corrected steady-state photoluminescence (PL) measurements were obtained with a fluorimeter (Spex Fluorolog) consisting of a single excitation monochromator (1681) optically coupled to a 450 W xenon arc lamp and a double detection monochromator (1682) with a GaAs photomultiplier tube (Hamamatsu). PL spectra were acquired at room temperature and were corrected for the wavelength-dependent system detection by calibration with a traceable, 45 W tungsten-halogen irradiance-standard lamp (Optronic Laboratories OL 245 M (NIST calibrated)).

Electrochemistry. A potentiostat (BAS model CV-50W or Epsilon electrochemical analyzer) was employed for measurements in a standard three-electrode arrangement with a sensitized TiO_2 thin film deposited on an FTO substrate working electrode, a Pt gauze or Pt disk (Bioanalytical Scientific Instruments, Inc.) counter electrode, and an aqueous Ag/AgCl (NaCl saturated) reference electrode (Bioanalytical Scientific Instruments, Inc.). All potentials are reported versus the normal hydrogen electrode (NHE) unless otherwise noted. The ferrocenium/ferrocene ($FeCp^{2+/+}$) half-wave potential measured in a 200 mM $LiClO_4$ acetonitrile electrolyte was used as a standard to calibrate the reference electrode, $E_{1/2}(FeCp^{2+/+}) = +447.1$ mV vs Ag/AgCl (NaCl saturated). Conversion to vs NHE was achieved using the published values for the reference electrode, i.e., + 197 mV vs NHE,[43] and correcting for the expected $E_{1/2}(FeCp^{2+/+})$ of +310 mV vs the KCl-saturated aqueous calomel electrode (SCE), where SCE is +241.2 mV vs NHE.[43]

Spectroelectrochemistry was performed via application of a potential bias concurrent with monitoring the UV−vis absorbance spectra of sensitized TiO_2 thin-film electrodes. After 1−2 min, a spectrum that was invariant with time was recorded and the process was repeated for subsequent potential biases. Single-wavelength absorbance features plotted as a function of potential bias were proportional to the cumulative formation/loss of states; for the $TiO_2(e^-)$ absorbance features this was directly related to the cumulative TiO_2 density of states in free energy.

Data Fitting. Kinetic data fitting and spectral modeling was performed in Origin 7.0, and least-squares error minimization was accomplished using the Levenberg−Marquardt iteration method. For the spectral modeling, a method for the standard addition of known spectra was developed using the C programming language and was implemented in Origin's error minimization routine.

Results

The pertinent di- and triimine ligands and ruthenium precursors were synthesized through adaptation of published procedures.[25−29] The heteroleptic sensitizer of mixed denticity, [Ru(^{t}Bu$_3$tpy)(dcb)(NCS)](PF$_6$), was readily obtained by a one-pot procedure developed for the preparation of Z907, *cis*-Ru(dcb)(dnb)(NCS)$_2$ (Scheme 2).[30,31] An alternative synthesis for the benchmark sensitizer N3, *cis*-Ru(dcb)$_2$(NCS)$_2$, was developed that did not require chromatography. The compound [Ru(dtb)$_2$(dcb)](PF$_6$)$_2$ (Scheme 2), was first isolated as its diethyl ester precursor, [Ru(dtb)(deeb)](PF$_6$)$_2$, and was subsequently saponified to the corresponding carboxylate compound in aqueous base. All of the newly synthesized compounds were characterized by ^{1}H and ^{13}C NMR in addition to MALDI-TOF mass spectrometry.

Figure 1 shows the absorption and photoluminescence (PL) spectra of [Ru(dtb)$_2$(dcb)](PF$_6$)$_2$ anchored to a mesoporous, nanocrystalline (anatase) TiO_2 thin film, abbreviated Ru(dtb)$_2$(dcb)/TiO_2, immersed in 100 mM $LiClO_4$ acetonitrile electrolyte. Also shown are the absorption and PL spectra of the same film in neat CH_3CN after thorough rinsing with acetonitrile, i.e., 10 times. In the presence of Li^+, both maxima red-shifted and their intensity decreased relative to neat acetonitrile. An approximate isosbestic point, ±1 nm, was maintained at 433 and 486 nm for the absorption data. Interestingly, at lower surface coverages these isosbestic points occurred at shorter wavelengths (Figure S1A, Supporting Information). This bathochromic shift was also observed upon addition of HCl, $Mg(ClO_4)_2$, $Cu(ClO_4)_2$, and $AgNO_3$, and to a much lesser extent 1-*n*-propyl-3-methylimidazolium iodide, guanidinium thiocyanate, and the ClO_4^- or Cl^- salts of *n*-tetrabutylammonium (TBA^+). The addition of Li^+ to an acetonitrile solution that contained either a SnO_2 or ZrO_2 thin film sensitized with [Ru(dtb)$_2$(dcb)]$^{2+}$ also induced a similar change in the sensitizer absorption spectrum. Related, although less-pronounced, Li^+-induced absorption changes were observed for the following sensitized thin films: Ru(bpy)$_2$(dcb)/TiO_2 where bpy is 2,2′-bipyridine, N3/TiO_2, Z907/TiO_2, Ru(^{t}Bu$_3$tpy)(dcb)(NCS)/TiO_2, Ru(bpy)$_2$(4-CH$_3$-4′-COOH-bpy)/TiO_2, Ru(deeb)$_3$/TiO_2, and Os(bpy)$_2$(deeb)/TiO_2. Unless noted otherwise, all experiments were performed with acetonitrile-based solutions.

The magnitude of the Li^+-induced spectral shift for Ru(dtb)$_2$(dcb)/TiO_2 thin films was quantified by titration experiments with $LiClO_4$. Difference spectra were calculated for each Li^+ concentration based on the spectrum measured in neat acetonitrile. The fractional spectral change measured at 505 nm was plotted as a function of the Li^+ concentration and was fitted to the Langmuir adsorption isotherm model, from which an adduct-formation constant was abstracted, 15−80 M^{-1} (Figure S1B, Supporting Information). When the spectrum in neat acetonitrile, or in the presence of trace Li^+, was plotted as a function of

(42) Qu, P.; Meyer, G. J. *Langmuir* **2001**, *17*, 6720–6728.
(43) Bard, A. J.; Faulkner, L. R. *Electrochemical Methods: Fundamentals and Applications*, 2nd ed.; John Wiley & Sons, Inc.: New York, 2001.

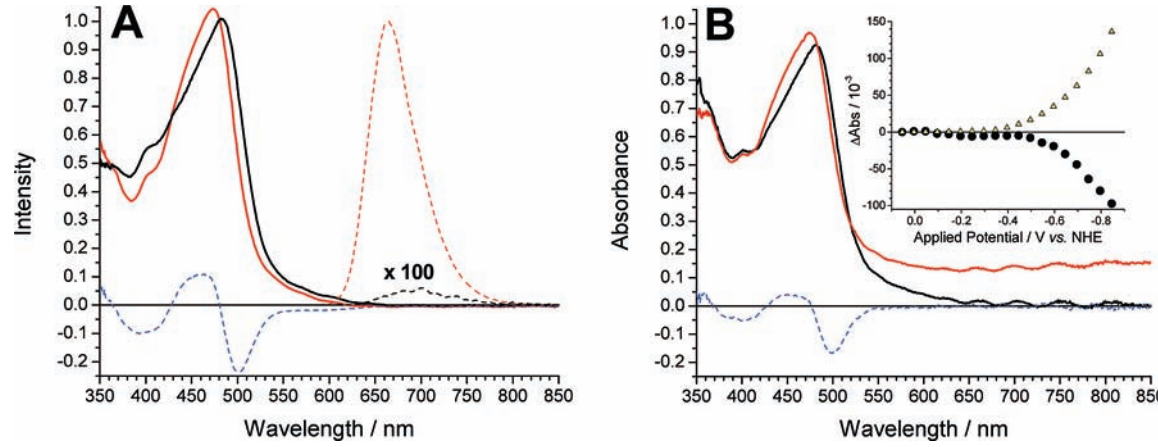

Figure 1. (A) Absorption and photoluminescence spectra of $[Ru(dtb)_2(dcb)]^{2+}$ anchored to a TiO_2 thin film immersed in 100 mM $LiClO_4/CH_3CN$ (black); in neat acetonitrile after removal of the $LiClO_4/CH_3CN$ solution and 10 acetonitrile washings (red); their difference spectrum (blue, dashed). (B) Absorption spectrum of $[Ru(dtb)_2(dcb)]^{2+}$ anchored to a TiO_2/FTO thin film electrode in 100 mM $LiClO_4/CH_3CN$ with 500 mM $TBAClO_4$ at open circuit (black) and biased to −0.85 V vs NHE (red); their difference spectrum corrected for the absorbance features due to $TiO_2(e^-)$s (blue, dashed). Inset: absorbance changes measured as a function of applied bias for the maximum bleach at 500 nm (circles) and $TiO_2(e^-)$s at 750 nm (open triangles). The bias was held at each potential for 1−2 min before each steady-state absorption measurement.

wavenumber, it could be deconvoluted with three overlapping Gaussian distribution functions (Figure S2A, Supporting Information). The absorption changes observed with increased Li^+ concentration were effectively modeled by shifts in these Gaussians (Figure S2B light green, Supporting Information), in accord with an underlying Stark effect.[44] The infrared spectrum of $Ru(dtb)_2(dcb)/TiO_2$ in neat acetonitrile displayed a characteristic ν_{COO} asymmetric stretch at 1613 ± 1 cm^{-1},[42] fwhm ≈ 40 cm^{-1}, while addition of $LiClO_4$ to the external acetonitrile solution led to no measurable spectral changes.

In a standard three-electrode cell containing 100 mM $LiClO_4$/500 mM $TBAClO_4$, application of a reverse bias positive of the resting equilibrium potential, i.e., the measured potential in the absence of bias which was routinely about −100 mV, of $Ru(dtb)_2(dcb)/TiO_2$/FTO but prior to sensitizer oxidation, resulted in small spectral shifts similar to those observed in the absence of a bias in 100 mM $LiClO_4$. Application of a forward bias, prior to sensitizer ligand reduction, resulted in reduction of the TiO_2 thin film, forming $TiO_2(e^-)$s, concomitant with spectral shifts opposite to those generated by Li^+ or reverse bias. These forward-bias, sensitizer-based spectral features maintained isosbestic points that were typically red-shifted by ∼10 nm from those observed in Li^+ titration experiments at open circuit (see the difference spectra in Figure 1b versus a). The bias-induced spectroscopic changes to the sensitizers were nonlinear in applied potential and in the concentration of $TiO_2(e^-)$s as determined from the change in absorbance at 750 nm (Figure 1b, inset) and were irreversible on the hours time scale even with the application of a positive applied bias. Such spectroelectrochemical behavior was also observed in the presence of acetonitrile electrolytes containing $TBAClO_4$ only; although then the spectral changes were reversible and the magnitude of the effect was less pronounced (data not shown).

Transient absorption spectra were recorded after pulsed 532 nm laser excitation of $Ru(dtb)_2(dcb)/TiO_2$ thin films immersed in 100 mM $LiClO_4$. Representative spectra are shown in Figure 2a at various delay times. Full spectra normalized at 433 nm recorded 88 and 1 μs after the laser pulse are shown as an inset in Figure 2b. Their difference spectrum is also depicted (orange), overlaid by a scaled version of the Li^+-induced difference spectrum from Figure 1a (blue, dashed). The long-time value of 88 μs was chosen as it (a) represented a time where a majority of the signal had decayed, (b) resulted in data that still had a significant signal-to-noise ratio for effective data analysis (>11 for the raw data and >5 for the normalized transients), and (c) was the longest time attainable with our oscilloscope at the highest digitizing rate.

Wavelength-dependent kinetics were clearly observed by comparison of absorption changes monitored at 510 nm (green; near the absorption maximum) and 433 nm normalized at 88 μs (violet; Li^+ isosbestic point from Figure 1), Figure 2b. The difference in these kinetic data was nonexponential but was well described by the Kohlrausch−Williams−Watts (KWW) model, eq 1:

$$I(t) = I_o \exp[-(t/\tau_o)^{\beta}] \quad (1)$$

Here, β is inversely related to the width of the underlying Lévy distribution of rate constants, $0 < \beta < 1$, and τ_o is a characteristic lifetime.[45] Best fits to this model yielded $\tau_o \approx 1.5 \times 10^{-6}$ s and $\beta \approx 0.40$. The same experiments and analyses were performed on $Z907/TiO_2$ thin films and the difference transient-absorption kinetic data that resulted exhibited indistinguishable kinetics on a logarithmic scale.

Shown in Figure 3 are transient absorption changes measured under conditions identical to that of Figure 2 except that for Figure 3a,b, 500 mM TBAI and 50 mM phenothiazine, PTZ, were included in the external acetonitrile solution, respectively, and $[Ru(bpy)_2(dcb)]^{2+}$ (Scheme 2) was employed as the sensitizer in Figure 3b. On the microsecond time scale shown only oxidized donors and $TiO_2(e^-)$s were expected to be observed as the sensitization cycle was complete. The oxidized iodide products absorb predominantly below 450 nm and the $TiO_2(e^-)$s absorb weakly across the entire visible region but are clearly observed at $\lambda > 600$ nm. The absorption spectrum of oxidized PTZ is shown as an inset. The large bleach observed at

(44) Oh, D. H.; Sano, M.; Boxer, S. G. *J. Am. Chem. Soc.* **1991**, *113*, 6880–6890.

(45) Xia, H.-L.; Ardo, S.; Narducci Sarjeant, A. A.; Huang, S.; Meyer, G. J. *Langmuir* **2009**, *25*, 13641–13652.

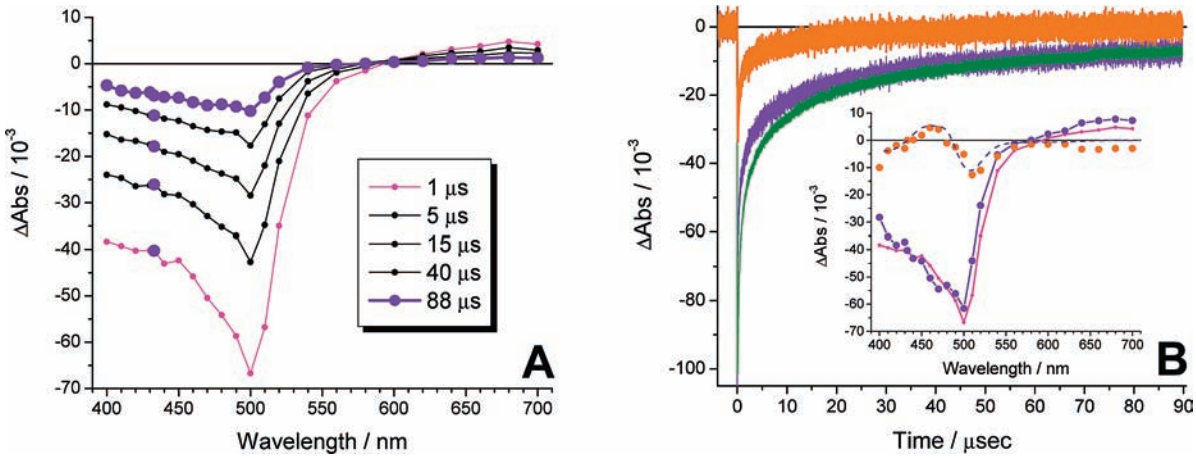

Figure 2. (A) Absorption difference spectra measured at the indicated delay times after pulsed 532 nm excitation of a $Ru(dtb)_2(dcb)/TiO_2$ thin film immersed in 100 mM $LiClO_4/CH_3CN$. The violet points represent those where exclusively $Ru^{III}(dtb)_2(dcb)/TiO_2(e^-)$ features are present. (B) Absorption change measured at 510 nm (green) and at 433 nm, normalized at 88 μs to the signal at 510 nm (violet), and their difference spectrum (orange). The inset displays spectra from panel A at 1 μs (magenta) and at 88 μs, normalized at 433 nm to the 1 μs spectrum (violet), and their difference spectrum (orange). Overlaid on the difference spectrum in the inset is the scaled difference spectrum shown in blue in Figure 1a.

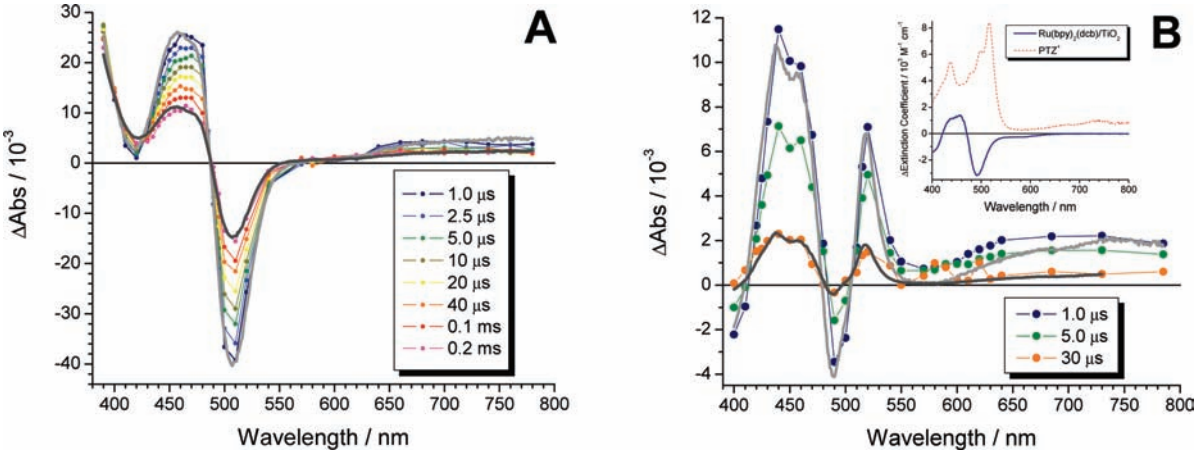

Figure 3. (A) Absorption difference spectra measured at the indicated delay times after pulsed 532 nm excitation of a $Ru(dtb)_2(dcb)/TiO_2$ thin film immersed in 100 mM $LiClO_4/CH_3CN$ with 500 mM TBAI. Overlaid on the shortest and longest time scale spectra are best-fit simulations of the data (gray). (B) Absorption difference spectra measured at the indicated delay times after pulsed 532 nm excitation of a $Ru(bpy)_2(dcb)/TiO_2$ thin film immersed in 100 mM $LiClO_4/CH_3CN$ with 50 mM phenothiazine (PTZ). Overlaid on the shortest and longest time scale spectra are best-fit simulations of the data (gray). Inset: difference extinction coefficient spectra for the Li^+-induced absorption changes of $Ru(bpy)_2(dcb)/TiO_2$ (blue) and the oxidation of PTZ to PTZ^+ (red, dashed).

~500 nm and the positive band at shorter wavelengths were unexpected and is the strongest evidence for the proposed Stark effect.

Spectral modeling of the transient absorption spectra was accomplished by standard addition of the absorption spectra of (1) $TiO_2(e^-)$s, (2) I_3^- (or PTZ^+), and (3) the absorption change measured in the absence and presence of 100 mM $LiClO_4$, e.g., for $Ru(dtb)_2(dcb)/TiO_2$, the red minus the black spectrum shown in Figure 1a which corresponded to a blue-shift of the original spectrum in the presence of Li^+. The corresponding extinction coefficient spectra for the sensitizers employed in this comparative study are presented in Supporting Information (Figure S3). Similar experiments were performed on each of the sensitized TiO_2 thin films that displayed Li^+-induced spectral changes mentioned above, and spectral modeling was able to satisfactorily reproduce the observed transient-absorption features. The stoichiometry of these three reaction products was calculated from the extinction coefficients and was found to be time dependent, indicating that at least two separate kinetic processes were associated with relaxation to the initial state. The excellent agreement between the observed spectra and the simulations in Figure 3a clearly highlights the fact that the (3)-to-(1) stoichiometry was greater than unity, i.e., 1.07 ± 0.05, at 1 μs delay times but decreased to 0.61 ± 0.03 at longer observation times (200 μs). For $Ru(bpy)_2(dcb)/TiO_2$ with PTZ as the donor, simulations revealed that the (3)-to-(1) stoichiometry decreased with time but was never less than unity, 2.86 ± 0.31 at 1 μs and 2.20 ± 0.39 at 30 μs. It should be noted that PTZ^+ absorbs more light across the visible region than does I_3^- or PTZ, and thus, it was more difficult to visually discern between the separate contributions from the Ru(II) sensitizers and PTZ^+ (Figure 3b, inset). Similar transient data was obtained for $Ru(dtb)_2(dcb)/TiO_2$, but the bleach at ~500 nm was not as directly apparent.

Spectral modeling of the transient absorption data required the use of isosbestic points and extinction coefficients determined from Li^+ titrations that differed significantly from those observed in spectroelectrochemical measurements. A possible source of error in the calculation of the concentration of the transient Ru(II) species arises from the fact that the Li^+-induced spectral changes did not fully saturate at the highest $LiClO_4$ concentrations that solubility allowed. By extrapolation of the

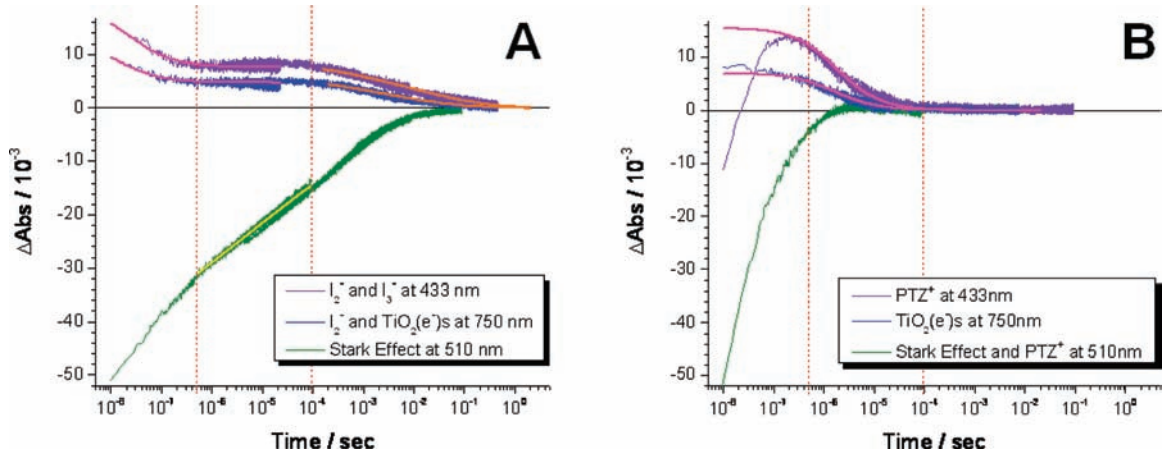

Figure 4. Transient absorption changes for a $Ru(dtb)_2(dcb)/TiO_2$ thin film immersed in 100 mM $LiClO_4/CH_3CN$ after pulsed 532 nm excitation monitored at 433 nm (purple), 510 nm (green), and 750 nm (blue) in the presence of (A) TBAI (500 mM) or (B) PTZ (50 mM) and $TBAClO_4$ (500 mM). An isosbestic point for the cation difference spectrum occurs at 433 nm, whereas a maximum bleach in the cation difference spectrum and a PTZ^+ growth occur near 510 nm. Spectral features due to $TiO_2(e^-)$s and oxidized iodide species, i.e., $I_2^{\bullet-}$, predominate the transient spectrum at 750 nm. Overlaid are fits to a second-order, equal-concentration (magenta) or KWW (orange and yellow) kinetic model. The red dashed lines are guides for the eye to highlight the same time domains on both graphs.

isotherm fits (Figure S1B, Supporting Information), the possible error propagated may have been upward of 10% if a final end point beyond the solubility limit of $LiClO_4$ in acetonitrile existed and the Langmuir fitting ranges were accurate. This would lead to an underestimation of the true Ru(II) concentration calculated at all delay times and a corresponding error in the stoichiometric ratios described above.

Shown in Figure 4 are representative kinetic data measured after pulsed 532 nm excitation of $Ru(dtb)_2(dcb)/TiO_2$ with iodide or neutral, organic PTZ donors under identical ionic strengths. With 100 mM $LiClO_4$/500 mM TBAI, the kinetics for the loss of oxidized iodide species and $TiO_2(e^-)$s were nonexponential and were best described as biphasic. The first phase followed a second-order, equal-concentration kinetic model assigned to $I_2^{\bullet-}$ disproportionation into I_3^- and I^-, with a rate constant of $4 \pm 2 \times 10^9$ M^{-1} s^{-1} under the assumption of a 10 μm thick film with 50% porosity (Figure 4a, magenta), which is in reasonable agreement with values found for said reaction in fluid solution and in TiO_2 mesopores.[46,47] The second, and slower, phase was attributed to recombination of $TiO_2(e^-)$s with I_3^- and could be modeled satisfactorily by the KWW function (Figure 4a, orange), $\tau_o \approx 6 \times 10^{-3}$ s and $\beta \approx 0.29$. In 100 mM $LiClO_4$/500 mM $TBAClO_4$/50 mM PTZ, the kinetics for the recombination of $TiO_2(e^-)$s with oxidized PTZ (PTZ^+) were adequately modeled as a second-order, equal-concentration process (Figure 4b, magenta), $1.2 \pm 0.2 \times 10^8$ M^{-1} s^{-1}. Regeneration by PTZ was not as rapid under these conditions, and the growth of PTZ^+ was clearly evident in the purple data on a submicrosecond time scale.

The absorption change monitored at 510 nm after pulsed 532 nm excitation of $Ru(dtb)_2(dcb)/TiO_2$ immersed in 100 mM $LiClO_4$/500 mM TBAI was analyzed in more detail on the time scale shown by the dotted lines in Figure 4a. The kinetic data was found to be excitation-wavelength independent and did not follow a first-order model but was well described by the KWW function, $\tau_o = 6.5 \pm 3.3 \times 10^{-6}$ s and $\beta \approx 0.14$ (Figure 4a, yellow). Similar transient-absorption kinetics were observed for $Z907/TiO_2$ thin films under the identical experimental conditions. For an overall comparison, the time required for the spectral phenomenon to decay to half of its original value, i.e., half-life ($t_{1/2}$), was determined for each kinetic process: $TiO_2(e^-) + PTZ^+$, $\sim 10^{-6}$ s; sensitizer Stark effect, $\sim 10^{-5}$ s; $TiO_2(e^-) + I_3^-$, $\sim 10^{-3}$ s. Interestingly in the presence of 500 mM TBAI and 500 mM $Mg(ClO_4)_2$, the concentration of the transient Ru(II) species was nearly time independent, i.e., displayed a plateau, on the 1−100 μs time scale (Figure S4, Supporting Information), behavior that was not observed when 500 mM $LiClO_4$ was used instead of $Mg(ClO_4)_2$.

Shown in Figure 5a are the absorption spectra of a TiO_2 thin film sensitized with $[Ru(dtb)_2(dcb)]^{2+}$, and then with $[Ru(dtb)_2(dcb)]^{2+}$ and Z907 (Scheme 2) in a 2.3:1 molar ratio, abbreviated $Ru(dtb)_2(dcb)$:$Z907/TiO_2$. The Z907 was selectively excited with <1 mJ/pulse (absorbed) of 683 nm light while the observed difference spectrum at 1 μs clearly displayed $[Ru(dtb)_2(dcb)]^{2+}$-based absorption features, Figure 5b, large growth at 460 nm and bleach at 510 nm, and a smaller feature at ~570 nm due to Z907. Overlaid on this data is a simulation based on the standard addition method described above.

Discussion

The results presented herein, as well as in previous studies by Staniszewski,[20] Durrant,[21] Kamat,[22] and Hagfeldt,[23] clearly indicate that the absorption spectra of surface-anchored molecular sensitizers are influenced by electrons injected into the metal oxide nanoparticle. The measured spectral responses are reminiscent of those observed previously by electro-absorption (Stark) spectroscopy.[48,49] The studies reported here focus mainly on $[Ru(dtb)_2(dcb)]^{2+}$- and *cis*-$Ru(dcb)(dnb)(NCS)_2$-sensitized nanocrystalline (~15 nm diameter, anatase) TiO_2 mesoporous (~50%) thin films immersed in Li^+-containing CH_3CN electrolytes, although other electrolytes, sensitizers, and metal oxides were examined to confirm generality. While Stark effects have been observed in semiconductor nanocrystallites[50−52] and Ru(II)/

(46) Gardner, J. M.; Abrahamsson, M.; Farnum, B. H.; Meyer, G. J. *J. Am. Chem. Soc.* **2009**, *131*, 16206–16214.
(47) Rowley, J.; Meyer, G. J. *J. Phys. Chem. C* **2009**, *113*, 18444–18447.
(48) Boxer, S. G. *J. Phys. Chem. B* **2009**, *113*, 2972–2983.
(49) Bublitz, G. U.; Boxer, S. G. *Annu. Rev. Phys. Chem.* **1997**, *48*, 213–242.
(50) Hilinski, E. F.; Lucas, P. A.; Wang, Y. *J. Chem. Phys.* **1988**, *89*, 3435–3441.

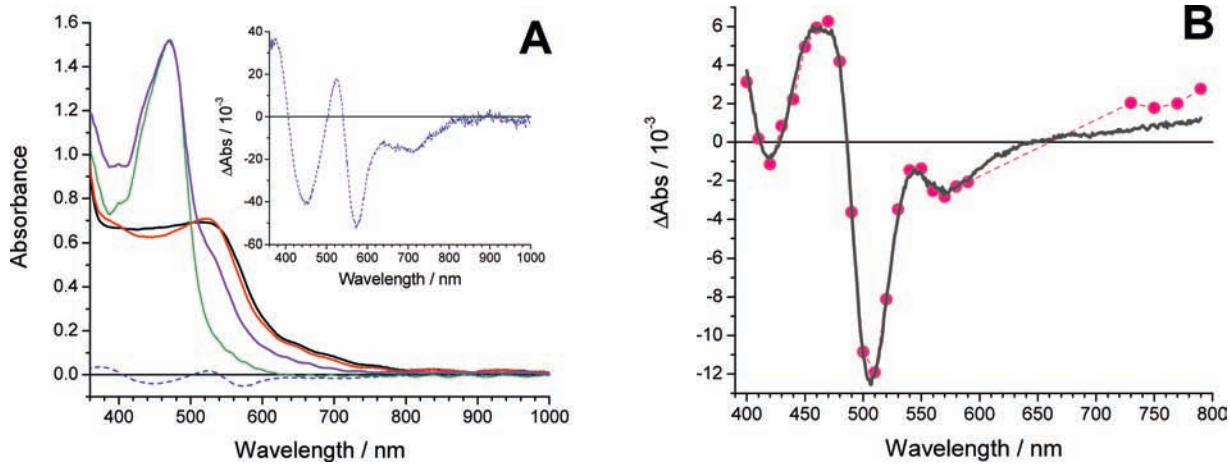

Figure 5. (A) Absorption spectrum of a TiO_2 thin film sensitized with $[Ru(dtb)_2(dcb)]^{2+}$ (green) and then $[Ru(dtb)_2(dcb)]^{2+}$/Z907 in a 2.3:1 molar ratio (violet). Also shown are the spectra of Z907/TiO_2 in acetonitrile in the presence (black) and absence (red) of 100 mM $LiClO_4$ and their difference spectrum (blue, dashed; expanded in inset). (B) Absorption difference spectrum measured at 1 μs delay time after pulsed 683 nm excitation of the cosensitized thin film from panel A in 100 mM $LiClO_4$/500 mM TBAI CH_3CN. Overlaid on the transient spectrum is a best-fit simulation of the data (dark gray).

Os(II) polypyridyl compounds,[53−61] they are not expected in dye-sensitized solar cells due to the high permittivity of TiO_2 and the high ionic strength electrolytes that are typically employed.[1,62−77] A working hypothesis emerged from the studies that is consistent with all experimental data yet is critically evaluated throughout this section, Scheme 3. This hypothesis begins with the assertion that electrons injected into TiO_2 produce an electric field. This field extends roughly normal to the semiconductor−sensitizer interface and induces a Stark effect on the sensitizer absorption spectrum. A kinetic competition then exists between ionic reorganization to shield this field, termed screening,[62,67,75] and interfacial charge recombination, magenta versus green arrows in Scheme 3. With PTZ donors, recombination was fast and screening was not clearly observed. On the other hand, with iodide donors, screening was observed prior to interfacial charge recombination, i.e., $TiO_2(e^-) + I_3^-$. To our knowledge, this was the first spectroscopic observation[20] and elucidation of an ionic screening process of the electric fields emanating from sensitized TiO_2 nanocrystallites. Although not shown in Scheme 3, the injected electron is found to perturb the absorption spectrum of multiple sensitizers, presumably those anchored to the same anatase nanocrystallite. The kinetics for screening as well as those for interfacial charge recombination were quantified and are discussed below.

Assignment as a Stark Effect. The origin of the observed spectral effect is clearly electron transfer to the semiconductor nanoparticles. Light absorption in the absence of electron transfer, observed when the TiO_2 acceptor states were energetically inaccessible or with insulating ZrO_2 nanoparticles, produced only the MLCT excited state that relaxed back to the ground state without any observable intermediates.[42,78] The large decrease in the PL intensity from the sensitizer with increased Li^+ concentration is due to electron transfer quenching by TiO_2.[79] The transient Stark effect was most clearly observed in the Ru(II) absorption spectrum after excited-state injection followed by regeneration with an electron donor but could also be observed transiently in the absence of electron donors (see below). Very similar behavior was induced by electrochemical reduction of the anatase nanocrystallites that comprise the mesoporous TiO_2 thin films. Once a steady-state concentration of electrons was present in a sensitized TiO_2 thin-film electrode a new time-independent electronic absorption spectrum was observed, indicating that the electric field was not completely screened from the sensitizer even with the high ionic-strength

(51) Norris, D. J.; Sacra, A.; Murray, C. B.; Bawendi, M. G. *Phys. Rev. Lett.* **1994**, *72*, 2612.
(52) Szczepankiewicz, S. H.; Moss, J. A.; Hoffmann, M. R. *J. Phys. Chem. B* **2002**, *106*, 7654–7658.
(53) Oh, D. H.; Boxer, S. G. *J. Am. Chem. Soc.* **1989**, *111*, 1130–1131.
(54) Karki, L.; Hupp, J. T. *Inorg. Chem.* **1997**, *36*, 3318–3321.
(55) Vance, F. W.; Hupp, J. T. *J. Am. Chem. Soc.* **1999**, *121*, 4047–4053.
(56) Hug, S. J.; Boxer, S. G. *Inorg. Chim. Acta* **1996**, *242*, 323–327.
(57) Riesen, H.; Krausz, E. *Chem. Phys. Lett.* **1996**, *260*, 130–135.
(58) Riesen, H.; Rae, A. D.; Krausz, E. *J. Lumin.* **1994**, *62*, 123–137.
(59) Riesen, H.; Krausz, E. *Chem. Phys. Lett.* **1993**, *212*, 347–352.
(60) Riesen, H.; Wallace, L.; Krausz, E. *J. Chem. Phys.* **1995**, *102*, 4823–4831.
(61) Riesen, H.; Wallace, L.; Krausz, E. *Int. Rev. Phys. Chem.* **1997**, *16*, 291–359.
(62) Gregg, B. A. *Coord. Chem. Rev.* **2004**, *248*, 1215–1224.
(63) Nelson, J. *Phys. Rev. B* **1999**, *59*, 15374.
(64) Schlichthorl, G.; Huang, S. Y.; Sprague, J.; Frank, A. J. *J. Phys. Chem. B* **1997**, *101*, 8141–8155.
(65) Schwarzburg, K.; Willig, F. *J. Phys. Chem. B* **1999**, *103*, 5743–5746.
(66) Dloczik, L.; Ileperuma, O.; Lauermann, I.; Peter, L. M.; Ponomarev, E. A.; Redmond, G.; Shaw, N. J.; Uhlendorf, I. *J. Phys. Chem. B* **1997**, *101*, 10281–10289.
(67) Zaban, A.; Meier, A.; Gregg, B. A. *J. Phys. Chem. B* **1997**, *101*, 7985–7990.
(68) Hendry, E.; Koeberg, M.; O'Regan, B.; Bonn, M. *Nano Lett.* **2006**, *6*, 755–759.
(69) Zaban, A.; Ferrere, S.; Gregg, B. A. *J. Phys. Chem. B* **1998**, *102*, 452–460.
(70) Gregg, B. A. *J. Phys. Chem. B* **2003**, *107*, 13540–13540.
(71) Könenkamp, R. *Phys. Rev. B* **2000**, *61*, 11057.
(72) Kytin, V.; Dittrich, T.; Bisquert, J.; Lebedev, E. A.; Koch, F. *Phys. Rev. B* **2003**, *68*, 195308.
(73) Hoyer, P.; Weller, H. *J. Phys. Chem.* **2002**, *99*, 14096–14100.
(74) Brus, L. *Phys. Rev. B* **1996**, *53*, 4649.
(75) Cahen, D.; Hodes, G.; Grätzel, M.; Guillemoles, J. F.; Riess, I. *J. Phys. Chem. B* **2000**, *104*, 2053–2059.
(76) Bisquert, J.; Cahen, D.; Hodes, G.; Ruhle, S.; Zaban, A. *J. Phys. Chem. B* **2004**, *108*, 8106–8118.
(77) Olson, C. L. *J. Phys. Chem. B* **2006**, *110*, 9619–9626.
(78) Kelly, C. A.; Farzad, F.; Thompson, D. W.; Meyer, G. J. *Langmuir* **1999**, *15*, 731–737.
(79) Kelly, C. A.; Farzad, F.; Thompson, D. W.; Stipkala, J. M.; Meyer, G. J. *Langmuir* **1999**, *15*, 7047–7054.

Scheme 3. Electric-Field Loss Mechanisms, as Indicated by the Transient Stark Effect, on Sensitized TiO_2 Nanocrystallites[a]

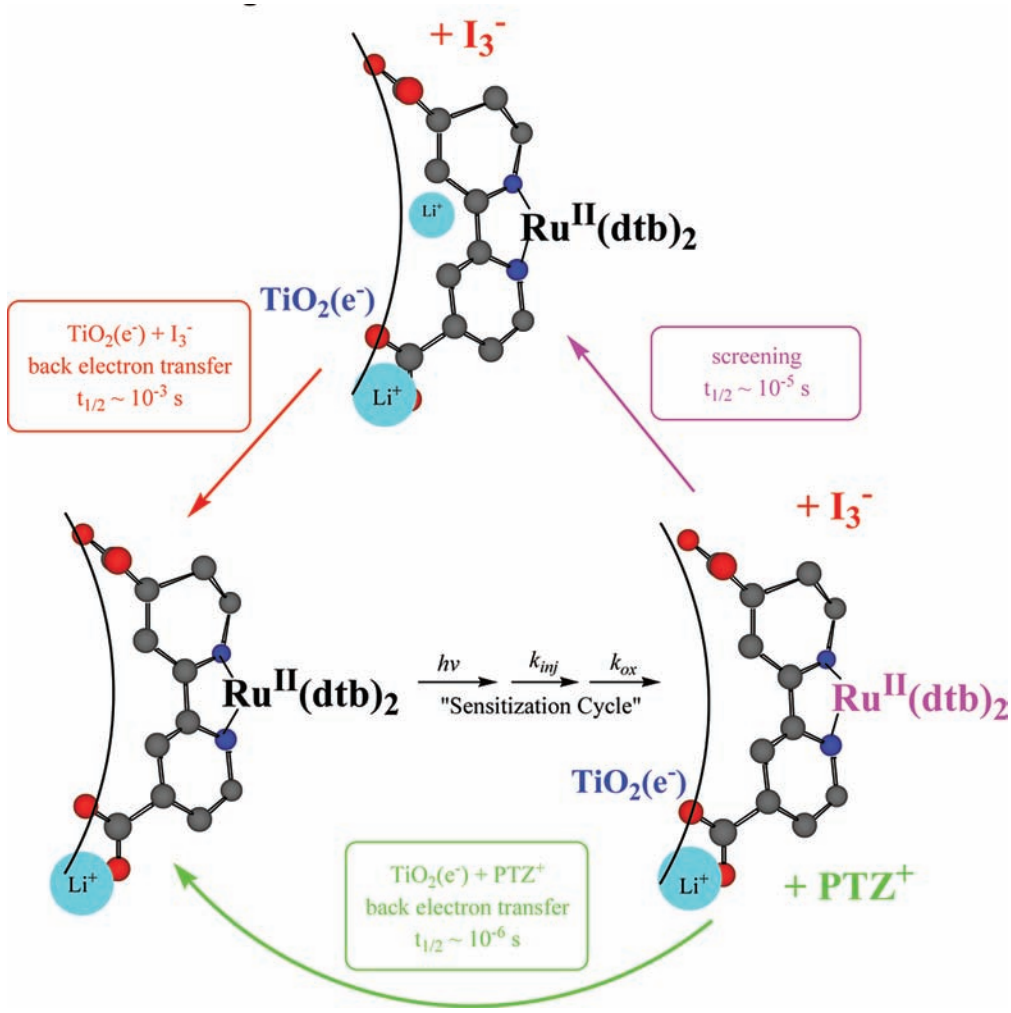

[a] After solvated Li^+ achieves adsorption equilibrium with sensitized TiO_2 nanocrystallites, pulsed-light excitation in the presence of electron donors results in the sensitization cycle (see Scheme 1). This yields a Ru(II) sensitizer whose absorption spectrum is perturbed by the injected electron, behavior that is attributed to a Stark effect. With phenothiazine donors, interfacial charge recombination directly yielded ground-state products. With iodide donors, charge recombination was slower, and a new dynamic process attributed to ionic reorganization, or "screening," was observed spectroscopically prior to interfacial electron transfer.

electrolytes employed, i.e., up to 600 mM, and the large relative permittivity of anatase TiO_2 ($\varepsilon_r = 7 - 50$)[80] and acetonitrile ($\varepsilon_r = 37.5$).[81]

Boxer and Oh first reported the electro-absorption (Stark) spectra of Ru(diimine)$_3^{2+}$ compounds,[53] and others have since studied related Ru(II) and Os(II) compounds.[54−61] These Stark spectra were generally obtained in amorphous solid-state media with application of a unidirectional electric field relative to the laboratory frame of reference. The orientation at these sensitized nanocrystalline thin films was different since the electric field was *not* unidirectional with respect to the laboratory frame of reference but extended normal to the TiO_2 surface toward the sensitizers and electrolyte. Macroscopically the field was isotropic; however, each field line had practically the same specific orientation relative to each individual sensitizer! Therefore, the physical interpretation of the observed spectral shifts differed from the usual analysis.

Stark spectra exemplify both changes in the extinction coefficient and energetic shifts in absorption maxima.[48,49] Variations in extinction coefficient, manifest as growths or losses in absorbance intensity, are due to electric field-induced changes in the transition moment *via* its influence on the transition polarizability $\underline{A}$ (linear in applied field) and hyperpolarizability $\underline{B}$ (quadratic in applied field). These represent scaled versions of the original spectrum. Transition peak position is altered by field interactions with the ground- and excited-state difference dipole moment $\Delta\vec{\mu}$ (linear in applied field) and polarizability $\underline{\Delta\alpha}$ (quadratic in applied field). Previous studies using Ru(II)-polypyridyl compounds, and specifically heteroleptic compounds like those investigated here, exhibit electro-absorption spectra almost entirely due to dipole moment changes.[53−61]

It is well-known that the broad nature of some transitions, like those observed for $Ru(dtb)_2(dcb)/TiO_2$, often lead to uncertainty in the absorption maxima. Therefore, the original absorption spectrum was modeled as a sum of three symmetric Gaussian absorption bands[44] in wavenumber space,[82] whose summation afforded increased precision of the band shape.[44]

(80) Olson, C. L.; Nelson, J.; Islam, M. S. *J. Phys. Chem. B* **2006**, *110*, 9995–10001, and references therein.
(81) *CRC Handbook of Chemistry and Physics*, 73rd ed.; CRC Press: Boca Raton, 1992.
(82) Parker, C. A.; Rees, W. T. *Analyst* **1960**, *85*, 587–600.

As is often the case, this accurately modeled the experimental data, with only minor deviations at the highest and lowest energy visible absorption features.[49] The sole goal of the Gaussian fits was to attain smooth spectra and was not intended to represent actual spectroscopic transitions in the $[Ru(dtb)_2(dcb)]^{2+}$ molecule. As can be seen, the spectrum in the presence of Li^+ is more effectively modeled by scaled shifts in these Gaussians as opposed to a global shift in the entire original absorption spectrum (Figure S2B, light green vs pink). However, as stated above, it is impossible to decipher the underlying physical mechanism without knowledge of the electric-field-strength dependence.

When in the presence of an electric field, the change in polarizability of the surface-bound molecules[54,83] should result in a bathochromic shift in the absorption spectrum,[48,49] contrary to what was observed. This suggests that the Stark effect here results predominately from changes in the sensitizer dipole moment. Oh and Boxer have calculated $|\Delta\vec{\mu}| \approx 4.75$ D for the lowest energy ^{1}MLCT transition of a related heteroleptic Ru(II)-polypyridyl compound.[53] This value, with the measured ~215 cm^{-1} bathochromic shift and an electric field oriented collinear with the direction of $\Delta\vec{\mu}$ for the sensitizer, implies an electric field intensity of ~270 MV/m.[84,85] Multiplication of this field value by the charge-transfer distance of 1.525 Å approximated for $Ru(bpy)_3^{2+}$,[53] results in an estimated potential drop of ~40 mV. Interestingly, Grätzel and colleagues reported a similar value of ~50 mV from electrophoretic measurements of sensitized colloidal TiO_2 in propylene carbonate electrolytes.[11]

In order for such large fields to persist at these sensitized semiconductor interfaces, effective screening must be absent. Attenuation of the bulk permittivity of solvents is known to occur by upward of an order of magnitude at interfaces and specifically for solvation of dipoles.[85−87] While a wide range of relative permittivities has been reported for anatase TiO_2,[80] it clearly does not shield charge as well as its rutile polymorph.[88] In addition, a small distance between the $TiO_2(e^-)$ and the sensitizer would inhibit substantial screening by TiO_2, acetonitrile, and Li^+. Taken together, the environments at these sensitized TiO_2 interfaces may explain the ineffective screening by the anatase lattice and acetonitrile electrolyte.

Aside from a Stark effect, another possible explanation for the observed spectral changes is that acid−base chemistry of the sensitizer accompanies TiO_2 reduction. In fact, *both* a Stark effect and acid−base chemistry may underlie the observed spectroscopic changes. It has been known for some time that reduction of TiO_2 results in cation adsorption onto the anatase surface.[11,13] Excited-state injection yields are often low in the absence of small "potential-determining cations", e.g., Li^+, H^+, Na^+,[79] and quartz crystal microbalance studies have shown that there is a 1:1 stoichiometry between adsorbed cations and electrochemically generated $TiO_2(e^-)$s.[89,90] Thus, it is not unreasonable that generation of the initial spectral changes could be due to nearby proton uptake by TiO_2, from the surface-anchored sensitizer, concurrent with $TiO_2(e^-)$ formation.

For the heteroleptic Ru(II) compounds, overlapping Ru → dcb and Ru → bpy (or dtb) metal-to-ligand charge transfer (MLCT) bands are evident. Charge transfer to the π^* orbitals of the dcb ligand occurs at lower energy due to the electron-withdrawing nature of the carboxylic acid groups. These functional groups are present in their carboxylate forms on the TiO_2 surface[42] and protonation or Li^+ interactions would red shift the MLCT absorption and PL.[42,79] With hard, Lewis-acidic cations like Li^+ or H^+, inner-sphere coordination to the carboxylic acid groups of the dcb ligands would influence the absorption spectrum in a predictable and known manner.[91−95] When the carboxylate forms of the sensitizers in solution were exposed to H^+ or Li^+, UV−vis absorption features similar to those observed for $Ru(dtb)_2(dcb)/TiO_2$ thin films were observed. However, infrared measurements in the COO stretching region for $Ru(dtb)_2(dcb)/TiO_2$ thin films displayed no significant spectral changes when Li^+ was introduced. Therefore, Li^+ does not appear to directly interact with the carboxylate groups of the sensitizers when they are anchored to TiO_2 thin films.[96] Notwithstanding, the cation reorganization proposed to accompany TiO_2 reduction may still perturb the sensitizer absorption spectrum through inner- and/or outer-sphere interactions. However, in the presence of *n*-tetrabutylammonium cations significant transient-absorption spectral features were observed even though such cations are not expected to have strong interactions with the carboxylate groups. Taken together, these findings support the assertion that the sensitizer spectral changes result from a Stark effect accompanied by outer-sphere or bulk screening.

Hagfeldt, Boschloo, and colleagues have also reported similar absorption changes after electrochemical reduction of related perylene-sensitized TiO_2 surfaces that were not intentionally exposed to small cations.[23] Under such conditions, screening should be minimal and the Stark effects most pronounced. Our results with Ru(II) sensitizers are in qualitative agreement with this. The absorption changes observed after sensitization have the same general shape and can be observed with an applied bias, albeit with unique isosbestic points. A consensus is that the sensitizers experience a significant electric field from the interface even at low concentrations of $TiO_2(e^-)$s.

Appearance of the Stark Effect. Since excited-state injection is known to occur on pico- to femto-second time scales under many conditions,[97−99] it was of interest to see if the Stark effect was present after electron injection yet before regeneration with an electron donor. In all previous work, the Stark effect was observed only after both excited-state injection and regeneration *or* in electrochemically reduced TiO_2 thin films where the formal oxidation state of the sensitizer had not changed. After excited-state injection, it was postulated that Stark effects should be present, Scheme 1, while the Ru formal oxidation state was Ru(III).

(83) Vance, F. W.; Williams, R. D.; Hupp, J. T. *Int. Rev. Phys. Chem.* **1998**, *17*, 307–329.
(84) Gosztola, D.; Yamada, H.; Wasielewski, M. R. *J. Am. Chem. Soc.* **1995**, *117*, 2041–2048.
(85) Lockhart, D. J.; Kim, P. S. *Science* **1992**, *257*, 947–951.
(86) Steffen, M. A.; Lao, K.; Boxer, S. G. *Science* **1994**, *264*, 810–816.
(87) Lockhart, D. J.; Kim, P. S. *Science* **1993**, *260*, 198–202.
(88) Kim, J.; Jung, H.; No, J.; Kim, J.-R.; Hong, K. *J. Electroceram.* **2006**, *16*, 447–451.
(89) Lyon, L. A.; Hupp, J. T. *J. Phys. Chem.* **1995**, *99*, 15718–15720.
(90) Lyon, L. A.; Hupp, J. T. *J. Phys. Chem. B* **1999**, *103*, 4623–4628.
(91) Ferguson, J.; Mau, A. W. H.; Sasse, W. H. F. *Chem. Phys. Lett.* **1979**, *68*, 21–24.
(92) Kirsch-De Mesmaeker, A.; Jacquet, L.; Nasielski, J. *Inorg. Chem.* **1988**, *27*, 4451–4458.
(93) Nazeeruddin, M. K.; Kalyanasundaram, K. *Inorg. Chem.* **1989**, *28*, 4251–4259.
(94) Shimidzu, T.; Iyoda, T.; Izaki, K. *J. Phys. Chem.* **1985**, *89*, 642–645.
(95) Giordano, P. J.; Bock, C. R.; Wrighton, M. S.; Interrante, L. V.; Williams, R. F. X. *J. Am. Chem. Soc.* **1977**, *99*, 3187–3189.
(96) Furube, A.; Katoh, R.; Hara, K.; Sato, T.; Murata, S.; Arakawa, H.; Tachiya, M. *J. Phys. Chem. B* **2005**, *109*, 16406–16414.
(97) Watson, D. F.; Meyer, G. J. *Annu. Rev. Phys. Chem.* **2005**, *56*, 119–156.
(98) Schwarzburg, K.; Ernstorfer, R.; Felber, S.; Willig, F. *Coord. Chem. Rev.* **2004**, *248*, 1259–1270.
(99) Anderson, N. A.; Lian, T. *Coord. Chem. Rev.* **2004**, *248*, 1231–1246.

A difficulty with testing this postulate is that Ru(III) tris-diimine compounds generally absorb very little visible light, especially when compared to the Ru(II) state. Nevertheless, after excited-state injection, careful absorption measurements showed clear evidence for wavelength-dependent kinetic behavior that was inconsistent with formation of a single interfacial charge-separated state, i.e., $Ru^{III}(dtb)_2(dcb)/TiO_2(e^-)$. The data revealed that in addition to this interfacial charge-separated state, the absorption spectra of other Ru(II) sensitizers was perturbed in a manner consistent with a Stark effect. Studies with the Ru(II) bis-diimine, bis-isothiocyanto sensitizer Z907 were also performed to test generality and examine whether the absorption spectrum of the oxidized sensitizer was influenced by the injected electron. This sensitizer absorbs red and near-infrared light more strongly in its oxidized form due to $NCS^- \rightarrow$ Ru(III) ligand-to-metal charge-transfer transitions.[100,101] Here, again, wavelength-dependent relaxation was marked and was consistent with an underlying Stark effect for Ru(II) sensitizers that did not undergo excited-state injection. Measurements in the near-infrared region, where the Ru(II) sensitizers absorbed little light were also wavelength dependent probably indicative of a Stark effect on the oxidized sensitizers. However, it was difficult to verify these spectral changes were those expected for the Ru(III) compounds upon Li^+ introduction due to the known instability of N3 and Z907.[31,102−104] Therefore, this will be the subject of future studies. Nevertheless, this demonstrated for the first time that excited-state injection perturbs the absorption spectrum of *other sensitizers that did not undergo photoinduced electron injection*.

To what extent does the electric field from the injected electrons influence neighboring sensitizers? In one extreme, the influence could be on a single sensitizer akin to the Coulomb trap model proposed by Tachiya and colleagues.[105,106] However, the studies employing sensitized TiO_2 in the absence of external donors support the hypothesis that an injected electron influences many sensitizers within the time resolution of our apparatus, i.e., <10 ns. In other words, the electric-field change induced by the injected electron is "felt" by at least one other sensitizer. Indeed, the spectral modeling with $Ru(bpy)_2(dcb)/TiO_2$ described above required that an injected electron influence 2−3 other sensitizers. It should be emphasized that the modeling was based on the assumption that a discrete number of Ru(II) sensitizers were maximally affected by the electric field and a different model wherein a smaller portion of the maximum field was experienced by a larger fraction of the sensitizers cannot be ruled out. Nevertheless, selective excitation studies of TiO_2 thin films sensitized with two different Ru(II) compounds, and the experiments in the absence of donor molecules, clearly demonstrated that electrons injected by one sensitizer influenced the absorption spectra of others. Taken together, there is no doubt that the electric field generated by excited-state injection is not localized to a single sensitizer.

Ionic Screening and Relaxation. In agreement with nonadiabatic electron-transfer theory under the Born−Oppenheimer approximation, excited-state electron injection is instantaneous on nuclear time scales and reorganization of solvent and ions occurs after electron transfer. Therefore, the sensitizer "feels" the field created by the injected electron most significantly at short observation times. The transient Stark effect observed was indeed largest immediately after pulsed-laser excitation, then decreased in amplitude, and returned to zero only when most of the injected electrons had recombined to the oxidized sensitizers or phenothiazine donors. By inspection, the signatures for charge recombination differed from those associated with the transient Stark effect. Although the influence of the transient $TiO_2(e^-)$ concentration on the magnitude of the Stark effect remains unknown, it is quite possible that the amplitude of the Stark effect simply reports on this concentration. The situation differed with iodide donors where a significant ∼100 μs time scale was observed where the Stark effect rapidly decayed but the $TiO_2(e^-)$ concentration remained unchanged, behavior that is attributed to interfacial ionic reorganization or "screening."

Another possible explanation for the disappearance of the Stark effect, while there was no change in the $TiO_2(e^-)$ concentration, also existed; the observed dynamics may have reported on quasi-Fermi level equilibration of the $TiO_2(e^-)$s within the thin film. The enormous surface area of these thins films resulted in significant light harvesting such that laser excitation did not uniformly excite sensitizers across the entire thickness of the film; hence, light absorption and the concentration of injected electrons decreased exponentially across the 10 μm thick mesoporous film. Diffusion of electrons from regions containing a high concentration of $TiO_2(e^-)$s would not change the total number of electrons probed (and hence their absorption) but may influence the magnitude of the electric field experienced by surface-anchored sensitizers. Although not unreasonable, this was ruled out based on the surface-coverage dependence that when normalized were, within error, the same.[20] Furthermore, 532 or 436 nm excitation of $Ru(dtb)_2(dcb)/TiO_2$ at near-maximum surface coverage resulted in a 50% change in the fraction of light absorbed, yet the normalized kinetics were entirely insensitive to this. Therefore, the dynamics observed with iodide donors on this time scale are not a result of equilibration of the $TiO_2(e^-)$ concentration within the mesoporous thin film and are instead reasonably attributed to screening by ionic reorganization.

The Kohlrausch−Williams−Watts (KWW) stretched-exponential function was found to accurately model the ionic screening observed in the presence of Li^+ and I^- on the ∼100 μs time scale for $Ru(dtb)_2(dcb)/TiO_2$. This function is commonly applied to dielectric relaxation/reorganization in a variety of solvents, glasses, and other disordered materials.[107−112] The parameters abstracted correspond to a large distribution of screening rate constants with a characteristic rate constant, τ_o^{-1}, of $\sim 1.5 \times 10^5$ s^{-1} and half-life, $t_{1/2}$, on the order of 10^{-5} s. There was much uncertainty in this value given the large fraction of rapid screening that occurred initially and the restricted time scale where screening could be cleanly observed. Mechanistically, it was not obvious why the time scale for screening was sluggish given the greater than half molar electrolyte present. The insensitivity of the rate constants to the sensitizer surface

(100) Tachibana, Y.; Moser, J. E.; Grätzel, M.; Klug, D. R.; Durrant, J. R. *J. Phys. Chem.* **1996**, *100*, 20056–20062.
(101) Das, S.; Kamat, P. V. *J. Phys. Chem. B* **1998**, *102*, 8954–8957.
(102) Cecchet, F.; Gioacchini, A. M.; Marcaccio, M.; Paolucci, F.; Roffia, S.; Alebbi, M.; Bignozzi, C. A. *J. Phys. Chem. B* **2002**, *106*, 3926–3932.
(103) Wolfbauer, G.; Bond, A. M.; MacFarlane, D. R. *Inorg. Chem.* **1999**, *38*, 3836–3846.
(104) Zabri, H.; Gillaizeau, I.; Bignozzi, C. A.; Caramori, S.; Charlot, M.-F.; Cano-Boquera, J.; Odobel, F. *Inorg. Chem.* **2003**, *42*, 6655–6666.
(105) Katoh, R.; Furube, A.; Barzykin, A. V.; Arakawa, H.; Tachiya, M. *Coord. Chem. Rev.* **2004**, *248*, 1195–1213.
(106) Barzykin, A. V.; Tachiya, M. *J. Phys. Chem. B* **2004**, *108*, 8385–8389.
(107) Lindsey, C. P.; Patterson, G. D. *J. Chem. Phys.* **1980**, *73*, 3348–3357.
(108) Jonscher, A. K. *Nature* **1974**, *250*, 191–193.
(109) Ngai, K. L.; Jonscher, A. K.; White, C. T. *Nature* **1979**, *277*, 185–189.
(110) Jonscher, A. K. *Nature* **1975**, *253*, 717–719.
(111) Jonscher, A. K. *Nature* **1977**, *267*, 673–679.
(112) Shlesinger, M. F.; Montroll, E. W *Proc. Natl. Acad. Sci. U.S.A.* **1984**, *81*, 1280–1283.

coverage or charge suggests that the sensitizers or their carboxylate groups do not play a significant role. It therefore appears that the metal-oxide surface and/or electrolyte transport within the mesopores underlie this characteristic microsecond time scale for Li^+ screening. Interestingly, screening by Mg^{2+} was also observed on this time scale and, although not as effective, it was more rapid (Figure S4, Supporting Information).

Implications for Solar Energy Conversion. The Stark effect may influence several processes in dye-sensitized solar cells: light absorption, excited-state injection, and sensitizer regeneration/recombination. This manuscript demonstrates that photogenerated $TiO_2(e^-)$s that have yet to be collected in the external circuit clearly influence the absorbance spectrum of other sensitizers. The measured blue shifts and decreases of the MLCT absorption are clearly undesirable for solar light harvesting. However, for sensitizers like N3 and Z907, the effect is quite small and would lead to an insignificant, <0.001% decrease in light harvesting at the power point under 1 sun of air-mass 1.5 irradiation. The Stark effect yields a Ru(II) absorption spectrum that is known to inject poorly when photoexcited.[79] Excited-state injection yields are also known to decrease with excitation irradiance, yet our understanding of the origin of this behavior is lacking.[79,113] The observations reported here suggest that Coulombic repulsion by injected electrons may be responsible. Durrant and co-workers have in fact shown that when the $TiO_2(e^-)$ concentration was increased, the half-life for recombination to the oxidized sensitizers increased by up to 7 orders of magnitude.[114] On the other hand, *complete shielding* by the supporting electrolyte would be expected to facilitate longer-lived charge-separated states between the $TiO_2(e^-)$s and oxidized sensitizers. Wasielewski and co-workers reported a molecular analogue where creation of a second charge-separated state decreased the lifetime of a previously formed charge-separated state.[115] The transient molecular electric field created by the first charge-separated state is in some ways synonymous to the sensitized interfaces studied here since the field from the $TiO_2(e^-)$s can assist recombination to an oxidized sensitizer.

With the nanosecond time resolution of these studies, the appearance of the Stark effect, like electron injection, could not be time-resolved but was clearly evident by wavelength-dependent transient-absorption spectral changes. In agreement with previous work, the overall time scales for complete charge recombination of the injected $TiO_2(e^-)$ were microseconds to PTZ^+,[116] tens of microseconds to milliseconds to the oxidized sensitizer,[79,114,116] and hundreds of milliseconds to I_3^-.[117−119] The dynamics of these recombination processes were generally in good agreement with previous studies, and existing models were used to quantify this data with no significant surprises.[13,63,120−122]

It is interesting to note, however, that regeneration by the organic donor PTZ yielded a $PTZ^+/TiO_2(e^-)$ charge-separated state that was actually shorter lived than the initially formed Ru(III)/$TiO_2(e^-)$ state. In other words, translation of the "hole" from the oxidized sensitizer to the organic phenothiazine donor enhanced interfacial charge recombination. This presumably occurred because of decreased driving force and/or diffusion of PTZ^+ relative to the surface-confined oxidized sensitizer.[123−131] Therefore, even though PTZ efficiently regenerated the sensitizer and created a mobile "hole" capable of diffusion to the counter electrode, the injected electron reduced PTZ^+ before it could escape the mesopores of the TiO_2 thin film.

The electric field at the TiO_2 interface may also help clarify why recombination to cationic one-electron acceptors, like PTZ^+ or the oxidized sensitizer, is much more rapid than to anionic triiodide. The few orders of magnitude slower recombination kinetics seen with anionic triiodide may result from Coulombic repulsion between $TiO_2(e^-)$s and I_3^-. Thus, the observed sluggish and *incomplete screening* of $TiO_2(e^-)$s may be beneficial and lessen the driving force for recombination to I_3^-. This may enable even longer lived charge-separated species, i.e., $TiO_2(e^-)$s and I_3^-, and improved open-circuit photovoltages.

In contrast, iodide donors increased the lifetime of the $TiO_2(e^-)$ charge-separated state by several orders of magnitude where the reorganization of the ions at the interface to more effectively screen the electric field could be observed. As mentioned above, attenuation of this screening rate may increase the lifetime of this charge-separated state even further; however, high ionic-strength electrolytes must still be employed. If the capacitance of the electrolyte were smaller than that of the nanoparticle film, a large and diffuse interfacial potential drop would lead to Fermi-level pinning (band-edge unpinning)[132−134] that would limit the open-circuit photovoltage irrespective of the potential of the solution redox mediator. Synonymous to increasing the width of the space-charge layer in a solid-state p−n junction solar cell, increasing the Debye length for screening should aid in the generation of even further spatially separated and longer-lived anionic species, i.e. $TiO_2(e^-)$s and I_3^-. Although speculative, the lethargic pace of this additional screening step may help explain why iodide is far superior to organic donors for redox mediation in dye-sensitized solar cells.

(113) Kay, A.; Humphry-Baker, R.; Grätzel, M. *J. Phys. Chem.* **1994**, *98*, 952–959.
(114) Haque, S. A.; Tachibana, Y.; Klug, D. R.; Durrant, J. R. *J. Phys. Chem. B* **1998**, *102*, 1745–1749.
(115) Debreczeny, M. P.; Svec, W. A.; Wasielewski, M. R. *Science* **1996**, *274*, 584–587.
(116) Argazzi, R.; Bignozzi, C. A.; Heimer, T. A.; Castellano, F. N.; Meyer, G. J. *J. Phys. Chem. B* **1997**, *101*, 2591–2597.
(117) Bauer, C.; Boschloo, G.; Mukhtar, E.; Hagfeldt, A. *J. Phys. Chem. B* **2002**, *106*, 12693–12704.
(118) Green, A. N. M.; Chandler, R. E.; Haque, S. A.; Nelson, J.; Durrant, J. R. *J. Phys. Chem. B* **2005**, *109*, 142–150.
(119) Clifford, J. N.; Palomares, E.; Nazeeruddin, M. K.; Grätzel, M.; Durrant, J. R. *J. Phys. Chem. C* **2007**, *111*, 6561–6567.
(120) Nelson, J.; Chandler, R. E. *Coord. Chem. Rev.* **2004**, *248*, 1181–1194.
(121) Nelson, J.; Haque, S. A.; Klug, D. R.; Durrant, J. R. *Phys. Rev. B* **2001**, *63*, 205321.
(122) Durrant, J. R.; Haque, S. A.; Palomares, E. *Coord. Chem. Rev.* **2004**, *248*, 1247–1257.
(123) Kuciauskas, D.; Freund, M. S.; Gray, H. B.; Winkler, J. R.; Lewis, N. S. *J. Phys. Chem. B* **2001**, *105*, 392–403.
(124) Clifford, J. N.; Palomares, E.; Nazeeruddin, M. K.; Grätzel, M.; Nelson, J.; Li, X.; Long, N. J.; Durrant, J. R. *J. Am. Chem. Soc.* **2004**, *126*, 5225–5233.
(125) Moser, J. E.; Grätzel, M. *Chem. Phys.* **1993**, *176*, 493–500.
(126) Lu, H.; Prieskorn, J. N.; Hupp, J. T. *J. Am. Chem. Soc.* **1993**, *115*, 4927–4928.
(127) Martini, I.; Hodak, J. H.; Hartland, G. V. *J. Phys. Chem. B* **1998**, *102*, 607–614.
(128) Wang, Y.; Hang, K.; Anderson, N. A.; Lian, T. *J. Phys. Chem. B* **2003**, *107*, 9434–9440.
(129) Gaal, D. A.; Hupp, J. T. *J. Am. Chem. Soc.* **2000**, *122*, 10956–10963.
(130) Yan, S. G.; Prieskorn, J. S.; Kim, Y.; Hupp, J. T. *J. Phys. Chem. B* **2000**, *104*, 10871–10877.
(131) Dang, X.; Hupp, J. T. *J. Am. Chem. Soc.* **1999**, *121*, 8399–8400.
(132) Fan, F. R. F.; Bard, A. J. *J. Am. Chem. Soc.* **1980**, *102*, 3677–3683.
(133) Bocarsly, A. B.; Bookbinder, D. C.; Dominey, R. N.; Lewis, N. S.; Wrighton, M. S. *J. Am. Chem. Soc.* **1980**, *102*, 3683–3688.
(134) Bard, A. J.; Bocarsly, A. B.; Fan, F. R. F.; Walton, E. G.; Wrighton, M. S. *J. Am. Chem. Soc.* **1980**, *102*, 3671–3677.

Conclusions

The experimental data provides compelling evidence that excited-state injection of electrons into TiO_2 nanocrystallites interconnected in a mesoporous thin film creates an electric field that perturbs the metal-to-ligand charge-transfer (MLCT) absorption spectra of Ru(II) compounds anchored to the same surface. Pulsed-laser excitation of the sensitized materials in the absence of external electron donors (or with the organic donor phenothiazine) resulted in the appearance of a Stark effect with maximum amplitude at the initial observation times that disappeared as the injected electrons underwent interfacial electron transfer to the oxidized sensitizers (or PTZ^+). Pulsed-light excitation with iodide donors also resulted in the prompt appearance of the Stark effect but a new dynamic process was observed where the Stark effect decayed without concomitant interfacial charge recombination. This dynamic process was attributed to ionic reorganization at the sensitized interface that more effectively screened the field from the sensitizers. The screening kinetics were nonexponential but were well modeled by the Kohlrausch−Williams−Watts function, which was originally implemented to characterize dielectric relaxation.[107−112] A characteristic screening time, τ_o, of $\sim 7 \times 10^{-6}$ s and distribution parameter, β, of ~ 0.14 was abstracted from fits of the experimental data. Studies of TiO_2 thin films sensitized with two different Ru(II) compounds demonstrated that the electric field created by excited-state injection from one sensitizer influenced the absorption spectra of other sensitizers that had not undergone photoinduced charge transfer. Complementary spectroelectrochemical measurements performed under steady-state conditions demonstrated that electrochemical reduction of TiO_2 also induced a shift of the MLCT absorption that was not fully screened by high ionic-strength acetonitrile solutions. These findings are at odds with the commonly held view that the surface electric fields are effectively screened by the large permittivity of TiO_2 and the high ionic strength electrolyte present in the mesopores.[1,62−77] Screening of the electric fields is expected to influence the lifetime of interfacial charge-separated states and hence the open-circuit photovoltage of regenerative dye-sensitized solar cells. Studies of this type are underway in our laboratories.

Acknowledgment. The JHU portion of the work was supported by the Division of Chemical Sciences, Office of Basic Energy Sciences, Office of Energy Research, U.S. Department of Energy (DE-FG02-96ER14662). We thank Darren Achey for his assistance with the ^{1}H NMR measurements. S. A. acknowledges a Johns Hopkins University Greer graduate student fellowship. The BGSU portion of the work was supported by the National Science Foundation (CHE-0719050) and the Air Force Office of Scientific Research (FA9550-05-1-0276).

Supporting Information Available: Li^+-induced Stark effect UV−vis absorption spectra as a function of surface coverage, an isotherm for these Li^+-induced changes, Gaussian and shifted/scaled spectral modeling of the Stark effects, extinction coefficient spectra, and transient absorption difference kinetics for the Stark effect in Li^+- or Mg^{2+}-based electrolyte. The complete ref 7 is also included. This material is available free of charge via the Internet at http://pubs.acs.org.

JA909781G